DISSERTATION

CONSTITUTIVE MODELING OF THE BIAXIAL MECHANICS OF BRAIN WHITE MATTER

Submitted by

Kevin M. Labus

School of Biomedical Engineering

Colorado State University

In partial fulfillment of the requirements

For the Degree of Doctor of Philosophy

Colorado State University

Fort Collins, Colorado

Summer 2016

Doctoral Committee:

Advisor: Christian M. Puttlitz

Seth Donahue
Paul Heyliger
Susan James

ABSTRACT

CONSTITUTIVE MODELING OF THE BIAXIAL MECHANICS OF BRAIN WHITE MATTER

It is important to characterize the mechanical behavior of brain tissue to aid in the computational models used for simulated neurosurgery. Due to its anisotropy, it is of particular interest to develop constitutive models of white matter based on experimental data in order to define the material properties in computational models. White matter has been shown to exhibit anisotropic, hyperelastic, and viscoelastic properties. The majority of studies have focused on the shear or compressive properties, while few have tested the tensile properties of the brain. Brain tissue has not previously been tested in a multi-axial loading state, even though *in vivo* brain tissue is in a constant multi-axial stress state due to fluid pressure, and data from uniaxial experiments do not sufficiently describe multi-axial stresses.

The main objective of this project was to characterize the biaxial tensile behavior of brain white matter via experimentation and constitutive modeling. A biaxial experiment was developed specifically for testing brain tissue. Experiments were performed at a quasi-static loading rate, and an Ogden anisotropic hyperelastic model was derived to fit the data. A structural analysis was performed on biaxially tested specimens to relate the structure to the mechanical behavior. The axonal orientation and distribution were measured via histology, and the axon area fraction was measured via transmission electron microscopy. The measured structural parameters were incorporated into the constitutive model. A probabilistic analysis was performed to compare the uncertainty in the stress predictions between models with and without

structural parameters. Finally, dynamic biaxial experiments were performed to characterize the anisotropic viscoelastic properties of white matter. Biaxial stress-relaxation experiments were conducted to determine the appropriate form of a viscoelastic model. It was found that the data were accurately modeled by a quasi-linear viscoelastic formulation with an isotropic reduced relaxation tensor and an instantaneous elastic stress defined by an anisotropic Ogden model. Model fits to the stress-relaxation experiments were able to accurately predict the results of dynamic cyclic experiments.

The resulting constitutive models from this project build upon previous models of brain white matter mechanics to include biaxial interactions and structural relations, thus improving computational model predictions.

ACKNOWLEDGEMENTS

This work could only be completed with the support of many individuals. I am especially grateful for the guidance of Christian Puttlitz, who has been an incredible mentor and friend. I would also like to thank my committee members Seth Donahue, Tammy Donahue, Paul Heyliger, and Susan James for their support and guidance. Finally, I am grateful for the continuous support, inspiration, and friendship of the OBRL team: Kirk McGilvray, Cecily Broomfield, Ben Gadomski, Nicole Ramo, Snehal Shetye, and Kevin Troyer.

TABLE OF CONTENTS

LIST OF TABLES

LIST OF FIGURES

LIST OF EQUATIONS

1. BACKGROUND

1.1 Brain Anatomy & Structure

1.1.1 General Anatomy

The neural tissue of the brain can be divided into two components: grey matter and white matter. Grey matter consists of a large number of neuronal cell bodies and has a pink-grey hue due to the presence of capillaries. Functionally, grey matter can be thought of as the signal processing tissue, while white matter provides the conduits for signal transmission. White matter contains relatively few neuronal cell bodies, but a high density of myelinated axons. Signals are sent through the axons of neurons between regions of the brain as well as between the brain and the peripheral nervous system. White matter gets its white color from myelin surrounding the axons. Figure 1.1 highlights many key regions of the brain discussed throughout this document. Axons in the corona radiata extend from the globus pallidus, radially outward to the grey matter of the cerebral cortex. The corpus callosum connects the two hemispheres of the brain and contains highly aligned axons.

The brain is surrounded and protected by the meninges, made up of three fibrous layers: the pia mater, the arachnoid mater, and the dura mater. The pia mater is a very thin membrane attached to the surface of the brain, following its folds and contours. The arachnoid mater is a web-like structure tethering the pia to the dura. The dura mater is a thicker tough membrane that lies closest to the skull. Cerebrospinal fluid, located in the subarachnoid space between the arachnoid mater and the pia mater, is a viscous fluid that mechanically cushions the brain. A network of capillaries penetrates the brain, passing through the pia mater.

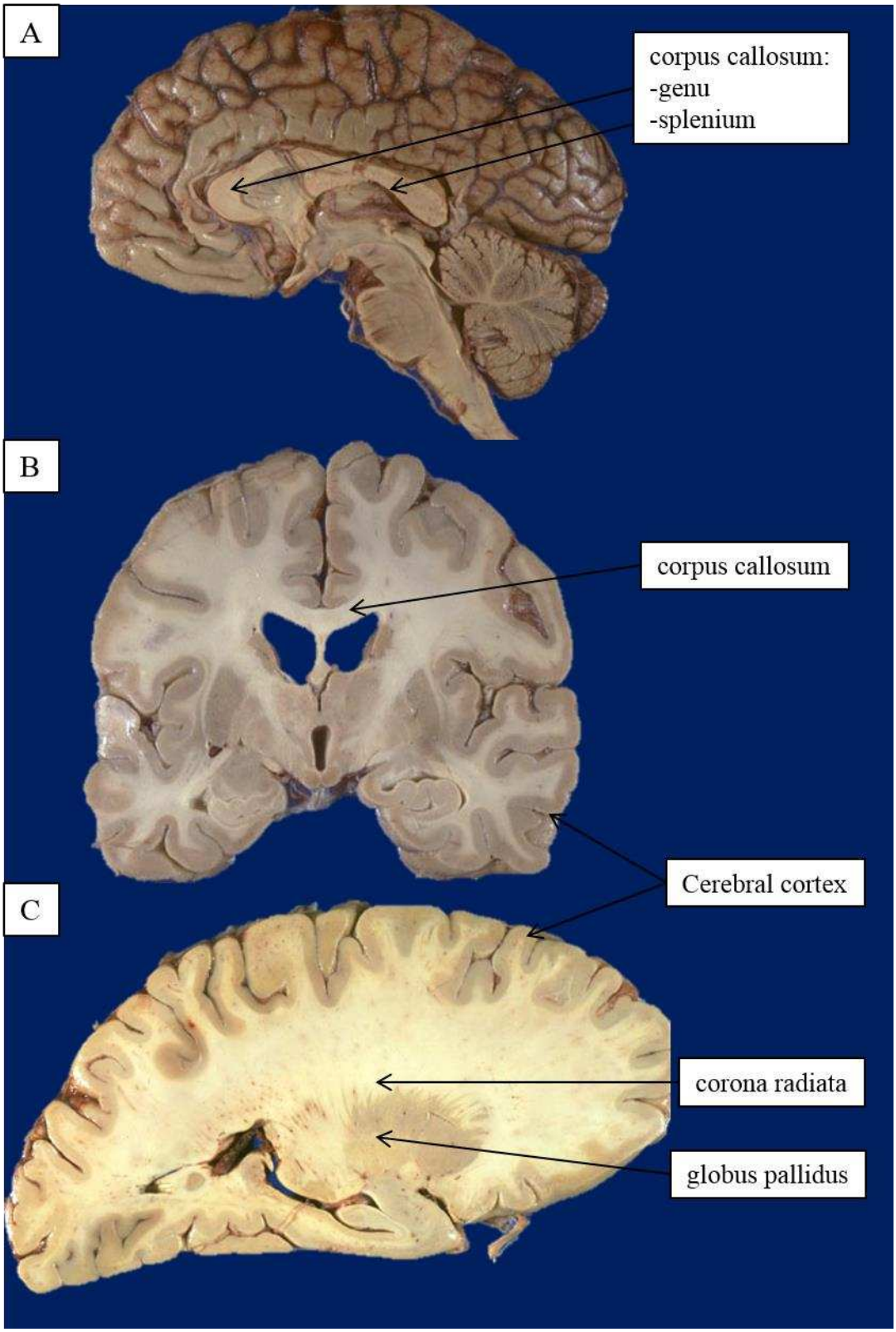

Figure 1.1: Anatomy of the brain shown in (A) mid-sagittal section, (B) coronal section, and (C) sagittal section in region of corona radiata (images adapted with permission from [The Internet Pathology Laboratory for Medical Education]).

1.1.2 Neurons

Neurons are the primary functional cells of nervous tissue, serving to transmit and process electrical signals via the movement of ions. Typical neurons consist of a soma (cell body), an axon, and dendrites (Figure 1.2). Signals are transmitted from the axon terminals of one neuron to the dendrites of another neuron via synapses. Most axons are surrounded by a myelin sheath, which provides electrical insulation. Myelin is made up of mostly lipids (70-85% of dry mass) as well as proteins (15-30% of dry mass) [Saher et al. 2005]. The nodes of Ranvier are gaps in the myelin sheath which contain voltage-gated ion channels. The myelin segments, combined with the nodes of Ranvier, allow for action potentials to jump from node to node, thus propagating the signal at faster speeds than an unmyelinated axon. Neurofilaments have a diameter of 10 nm and are the primary constituent of the neuron cytoskeleton [Yuan et al. 2012]. They provide structural support to axons to maintain their shape and diameter. The size of axons is highly variable, with the length ranging from less than 1 mm for interneurons, to greater than 1 m in the peripheral nervous system [Debanne et al. 2011]. In mammals, the myelinated axon diameter can range from about 1 µm up to 20 µm, with larger diameter axons allowing for faster signal conduction [Hursh 1939]. Unmyelinated axons are typically smaller, ranging from about 0.1-1 µm [Wang et al. 2008].

1.1.3Glial cells

Most other cells in nervous tissue are categorized as glial cells, named for being the 'glue' of nervous tissue. In the brain, the three main types of glial cells are astrocytes, microglia, and oligodendrocytes (Figure 1.2). Astrocytes are star-shaped cells that function as chemical regulators. They have processes that surround neuronal synapses, as well as processes that connect with endothelial cells on blood vessels. Microglia respond to foreign bodies and

changes in extracellular ion concentrations, and they act as the primary immune defense of the brain. Oligodendrocytes function to form the myelin. They contain processes that extend to axons, surrounding the myelin sheath. Oligodendrocyte-axon connectivity may play a role in the mechanical behavior of brain tissue. Axons with increased myelination have showed a greater kinematic affinity to the glial matrix [Hao and Shreiber 2007]. Additionally, white matter tensile stiffness is decreased by the disruption of myelination by oligodendrocytes, which is thought to be due to the decreased oligodendrocyte-axon connectivity rather than the decrease in myelin [Shreiber et al. 2009].

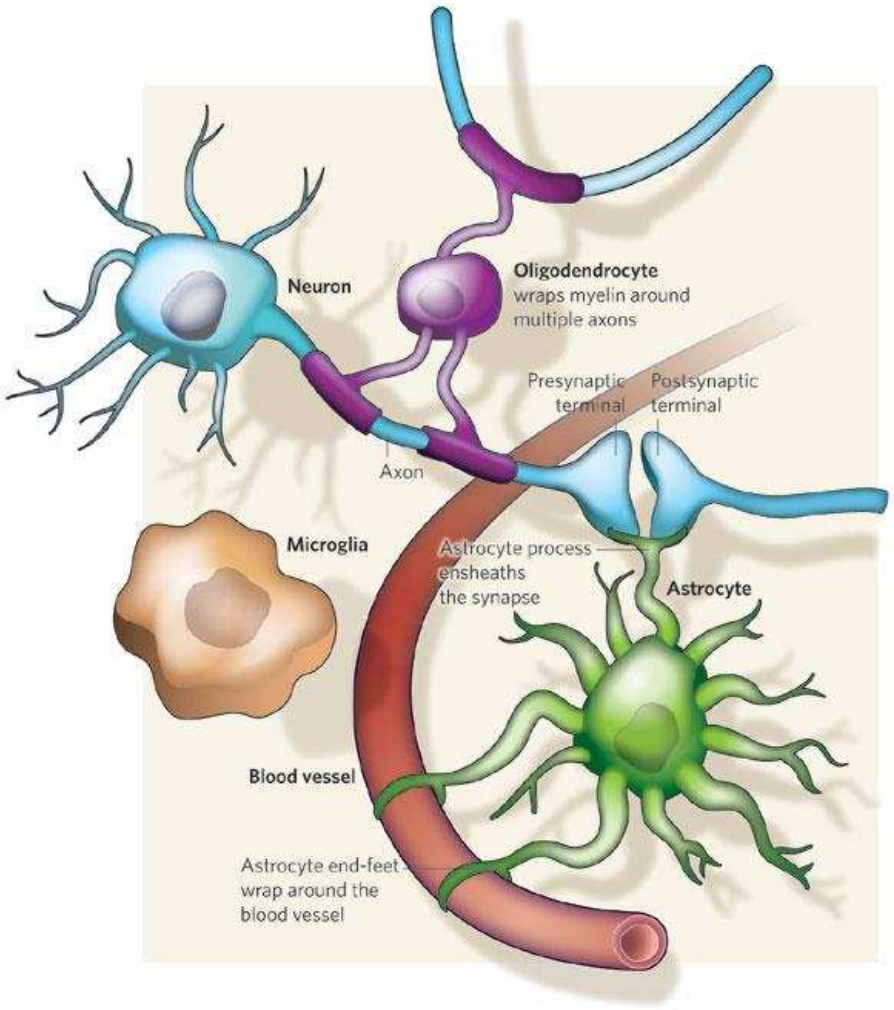

Figure 1.2: Diagram showing the morphology and interconnectivity of neurons and glial cells. Figure used with permission from [Allen and Barres 2009].

1.1.4 Extracellular Matrix

The extracellular space takes up about 17-20% of the brain volume [Cragg 1979]. The extracellular constituents include dense networks of proteoglycans, hyaluronan, and link proteins, the adhesive glycoproteins laminin and fibronectin, and small amounts of the fibrous proteins collagen and elastin [Lau et al. 2013]. In white matter specifically, hyaluronan and chondroitin sulphate proteoglycans are primary constituents found in the space between axons and in the nodes of Ranvier, and chondroitin sulphate proteoglycans aid in myelination [Asher et al. 1991, Lau et al. 2013]. While the extracellular matrix can aid in the myelination, and its hydrophilic nature can lead to increased hydration, it is not thought to provide structural support, and has been largely ignored in studies of mechanics.

1.2 Computational Modeling

It is important to study the mechanical behavior of brain tissue to incorporate the results into computational models. In turn, the models can be used for simulated neurosurgery, as well as the study of traumatic brain injuries. Experiments in the current study are motivated by computational models for simulated neurosurgery. Specifically, these models are useful for the development of surgical procedures, surgeon training, operation planning, and image registration to account for intraoperative brain shifts [Miller 2011, Ferrant et al. 2001]. Examples of surgical procedures include craniotomies, tumor debulking, and needle injections for drug delivery [Chan et al. 2013]. Computational models require accurate constitutive descriptions of the stress-strain relationship to compute the finite deformations that occur during operations [Garcia et al. 2012] as well as the force-feedback on the surgical tools [Chan 2013]. Due to the relatively low loading rates, the majority of models utilize constitutive equations based on quasi-static

experiments. However, viscoelastic effects are still important at low strain rates, and viscoelastic models have been recommended to improve the model predictions [Kyriacou et al. 2002].

The accuracy of computational models depends on the geometry, boundary conditions, and material definitions. Computational models of the brain differ in how the materials are defined. Grey matter and white matter are usually given different material properties, which have included isotropic linear viscoelastic properties based on in vitro shear experiments [Post et al. 2012, Zhang et al. 2001]. Other approaches have modeled the anisotropy of white matter and defining the axonal orientation based on diffusion tensor imaging [Colgan et al. 2010, Wright and Ramesh 2012]. Significant differences in predicted strains for some white matter regions have been reported when comparing models with anisotropic and isotropic material definitions [Colgan et al. 2010]. It has similarly been found that the orientation of axons affects the model predictions [Wright and Ramesh 2012].

1.3 Brain Mechanics

It is of particular interest to develop constitutive models to describe the mechanical behavior of brain tissue by fitting the models to experimental data.

1.3.1 In Vivo vs. in Vitro Experiments

It is generally desired for mechanical properties of biological tissues to be obtained *in vivo* in order to test the tissue in its natural state, in which the tissue is intact, perfused with blood, and temperature regulated. There are established techniques for *in vivo* determination of the mechanical behavior of the brain, but they do have some limitations. Ultrasound techniques estimate the complex shear and elastic moduli by measuring the attenuation and speed of high frequency sound waves propagating through the tissue [Lippert et al. 2004]. However, the depth of penetration is limited due to high attenuation through the skull, and the analysis is complicated

by inhomogeneous tissues [Cheng et al. 2008]. Magnetic resonance elastography is a similar technique in which mechanically-produced acoustic strain waves propagate through the tissue. The waves are measured using magnetic resonance imaging and analyzed to compute the complex shear modulus [Manduca et al. 2001]. This technique has the potential to measure anisotropy and detect differences in inhomogeneous tissues. Likewise, it has been used to compute the complex shear modulus of grey matter and white matter [Manduca et al. 2001, Green et al. 2008]. However, measurements are limited for deep tissues due to attenuation [Cheng et al. 2008]. Both ultrasound and magnetic resonance elastography are limited to studying small strains, and they do not test all deformation modes (tension, compression, and shear).

In vitro mechanical tests have the disadvantage of removing the tissue from its natural state, which can result in errors due to sample preparation, tissue degradation, and loss of perfusion. However, *in vitro* studies are more versatile and less complicated than *in vivo* studies because they do not require live subjects. More sophisticated experimental setups can be used in *in vitro* environments. Indentation stress-relaxation tests on porcine brains have been used to directly compare *in vivo*, *in situ* (no perfusion), and *in vitro* (brain not constrained within skull) setups [Gefen and Margulies 2004]. The only significant difference from *in vivo* to *in situ* setups was a decrease in the long term time constant. However, when removed from the skull, the computed shear modulus was significantly decreased from *in vivo* and *in situ* setups to *in vitro*. The altered boundary conditions that are requisite for *in vitro* testing may affect the measured mechanical properties, contributing to the high variability in published properties (for example, shear modulus values range from about 100 Pa to 10,000 Pa) [Hrapko et al. 2008].

1.3.2 Challenges in Mechanically Testing Brain Tissue

Mechanically testing brain tissue presents many challenges. Brain tissue is very soft and compliant. Very small forces are capable of causing damage. Therefore, care must be taken when handling the tissue and performing dissection. Handling procedures must be developed and followed to ensure the tissue remains undamaged at every step. The softness of the tissue also creates challenges for gripping. Some common gripping techniques used for other biological tissues, such as sutures and clamps, result in tears and do not effectively hold the tissue. The solution to effective gripping depends on experimental setup and boundary conditions (e.g. tension, compression, or shear). Some success has been found using adhesives [Miller and Chinzei 2002, Rashid et al. 2014], although adhesives have the potential to seep into the tissue, altering the mechanical behavior near the grip. In shear tests, specimens have been held between rough sandpaper surfaces along with a compressive preload to prevent slipping [Feng et al. 2013].

Another challenge in mechanically testing brain tissue is the rapid degradation of neural tissue post-mortem. The structure can be altered as a result of freezing and thawing the tissue, and even when fresh, the tissue begins to become stiffer after about six hours post-mortem [Garo et al. 2007]. It may be possible to slow degradation and extend this window by storing the tissue at low temperatures, but without freezing, between harvest and testing [Van Dommelen et al. 2010, Nicolle et al. 2004]. The short window of time limits the potential to test fresh human tissue. Accordingly, the large majority of mechanical experiments have used animal tissue.

1.3.3 Shear

It has been postulated that shear strain could correlate with the probability of a brain injury [Holbourn 1943]. Likewise, shear has been the most common form of mechanical tests on

brain tissue. Generally, blocks of tissue are dissected out and placed between two platens to be deformed in shear. Many studies have performed oscillatory shear tests at a range of frequencies to determine the linear viscoelastic properties (storage and loss modulus) at small strains [Abrogast and Margulies 1999, Feng et al. 2013, Nicolle et al. 2004, Garo et al. 2007]. While the reported moduli vary widely across these studies, they all show increasing storage and loss moduli as frequency increases [Hrapko et al. 2008]. Other studies have extended this work to large strains. Brain tissue has been deformed with shear strains up to 0.45 without damage being observed [Hrapko et al. 2006]. Nonlinear constitutive models are used to describe the stress-strain relationship at large strains [Prange and Margulies 2002, Ning et al. 2006], and many of these shear experiments have also found anisotropic behavior in white matter [Feng et al. 2013, Ning et al. 2006, Prange and Margulies 2002].

1.3.4 Compression and Indentation

Experiments investigating the compressive properties of brain tissue often utilize unconfined compression to achieve more reliable results and simplify the analysis compared to confined compression. The frictionless boundary condition is usually achieved using lubricants on the loading plates, although at high strain rates, the friction is not negligible, even with a lubricant [Rashid et al. 2012]. Studies that analyzed the stress-strain relationship consistently found a nonlinear behavior, with the tissue stiffening as strain is increased [Laksari et al. 2012, Miller and Chinzei 1997, Prevost et al. 2011, Rashid et al. 2012]. Viscoelastic properties are also investigated via stress relaxation and varying strain rates. Brain tissue has been shown to be consistently stiffer at higher strain rates [Miller and Chinzei 1997, Rashid et al. 2012]. However, there are contradictions on strain dependence, with some results showing quasi-linear viscoelasticity to be valid [Laksari et al. 2012], and other results requiring nonlinear viscoelastic

models to better fit the data [Prevost et al. 2011]. Another approach used a poroviscoelastic model and found that the tissue permeability affected the stress response [Cheng and Bilston 2007].

Indentation tests have the advantage of being able to localize the analysis to small regions. Specifically, results have found that white matter has a greater stiffness than grey matter, as well as greater variability in reported mechanical parameter data [Van Dommelen et al. 2010]. Indentation is also relatively non-invasive, and has been used to mechanically test brain tissue *in vivo* in animals by opening up the skull [Miller et al. 2000, Gefen et al. 2003, Gefen and Margulies 2004]. Similar to compression results, the stress-strain relationship in indentation is nonlinear, with the material stiffening at higher strains [Miller et al. 2000]. In stress-relaxation experiments using multiple strain magnitudes, it was found that quasi-linear viscoelasticity may be appropriate to model large strains in indentation [Elkin et al. 2011].

1.3.5 Tension

Relatively few studies have investigated the tensile properties of brain tissue. The studies differ in specimen gripping methods (Figure 1.3), with one method using an adhesive to attach each end of the specimen to a plate and pulling the plates in tension [Miller and Chinzei 2002, Rashid et al. 2014]. In this setup, the specimen width was greater than its length, creating inhomogeneous stresses and complicating the analysis. Another setup used long, thin specimens that were clamped at either end, allowing for a more simplified analysis, although boundary effects may arise due at the clamps [Velardi et al. 2006]. The shape of the stress-strain curve varies in tension between studies. One study reports curves that are very close to linear [Velardi et al. 2006], one reports a concave down shape which is especially pronounced at low strain rates [Miller and Chinzei 2002], and one reported a concave up shape [Rashid et al. 2014]. Another

study that loaded specimens cyclically in tension and compression showed a concave down behavior if loaded in tension first, but concave up if loaded in compression first (Figure 1.4) [Franceshini et al. 2006]. The tensile stiffness increases as strain rate increases [Miller and Chinzei 2002, Rashid et al. 2014], and when loaded to failure at a quasi-static strain rate, mechanical damage was reported to occur at a mean stretch of 1.9 [Franceshini et al. 2006].

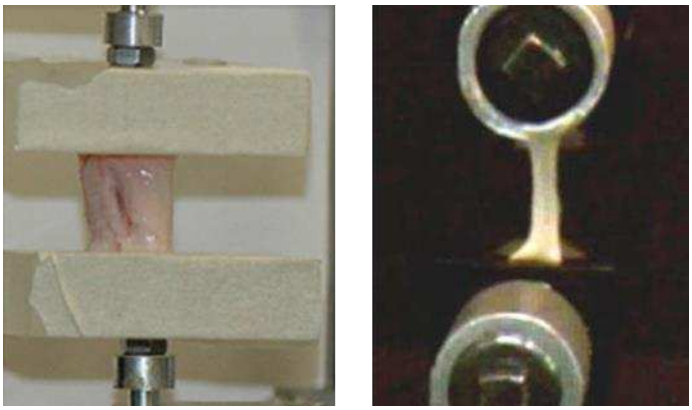

Figure 1.3: Tensile testing methods include using an adhesive to attach the specimen to two loading surfaces (left, adapted with permission from [Rashid et al. 2014]), and clamping the tissue at either end (right, used with permission from [Velardi et al. 2006]).

1.3.6 Stress-Strain Relationship

Many studies have attempted to determine the mechanical properties of brain tissue experimentally. Brain tissue is a very soft, easily deformed material. The infinitesimal shear modulus is a common measure reported in many methods of mechanical testing, and has been found to range from 0.13 kPa to 14 kPa in the reviewed literature [Velardi et al. 2006, Manduca et al. 2001]. Differences in the measured behavior may arise due to differences in preloads, temperature, testing protocols, and tissue donors [Hrapko et al. 2008]. The form of the stress-strain relationship depends on the mode of deformation. Compression exhibits a hyperelastic behavior in which the stiffness increases at higher compressive strains, but in shear, the stiffness

generally decreases as strain increases (Figure 1.5) [Prange and Margulies 2002, Hrapko et al. 2006]. However, in tension the shape of the stress-strain curve is inconsistent, but appears to depend on loading history [Franceschini et al. 2006] as well as strain rate [Miller and Chinzei 2002].

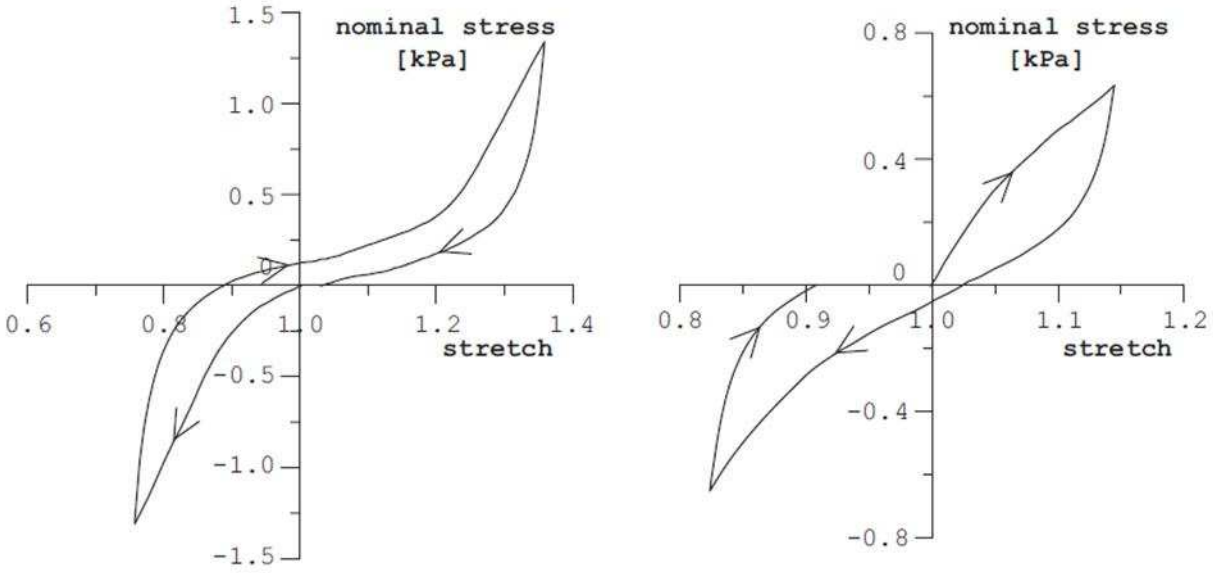

Figure 1.4: Brain tissue tested in compression and tension consistently shows a hyperelastic strain-stiffening behavior in compression. However, in tension, the behavior depended on whether the tissue was loaded in compression first (left) or tension first (right). Adapted with permission from [Franceschini et al. 2006].

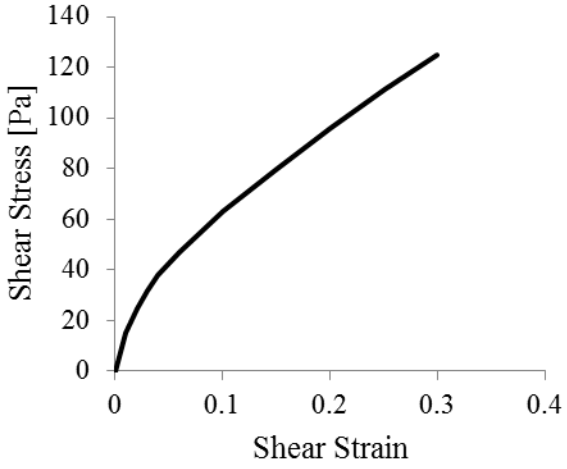

Figure 1.5: The stress-strain relationship of brain tissue in shear shows a concave-down curve. Figure created based on published data from [Hrapko et al. 2006].

1.3.7 White Matter vs. Grey Matter

Regional differences in mechanical properties have also been investigated, especially when comparing white matter and grey matter. Unfortunately, the results have been inconsistent. Some results from *in vitro* shear experiments found grey matter to be stiffer than white matter [Nicolle et al. 2004, Prange and Margulies 2002], although in one study, they were similar at small strains [Nicolle et al. 2004]. In one experiment in tension [Velardi et al. 2006] and one in indentation [Van Dommelen et al. 2010], white matter was found to be stiffer. Inconsistencies have even been found in two *in vivo* studies using the same technique. Using magnetic resonance elastography, one group found the shear modulus of white matter (14.2 kPa) to be significantly stiffer than grey matter (5.3 kPa) [Manduca et al. 2001], but another group found the shear modulus of grey matter to be significantly greater than for white matter (3.1 kPa and 2.7 kPa, respectively) [Green et al. 2008]. One consistent finding is that grey matter exhibits isotropic behavior [Prange and Margulies 2002, Shuck and Advani 1972, Feng et al. 2013], whereas white matter tends to be anisotropic [Velardi et al. 2006, Prange and Margulies 2002, Feng et al. 2013, Ning et al. 2006].

1.3.8 White Matter Anisotropy

Basic structural observations clearly show a directional alignment of axons in white matter. Diffusion tensor magnetic resonance imaging has been used to map the axonal tracts in white matter (Figure 1.6) and calculate measures of fractional anisotropy [Catani et al. 2002, Wakana et al. 2004]. In addition to structural alignment, experiments have shown white matter to exhibit mechanical anisotropy (Figure 1.7), but the degree of anisotropy is region dependent. In shear, the corpus callosum and corona radiata were both shown to be anisotropic [Prange and Margulies 2002]. As expected, the corpus callosum exhibited a greater stiffness in the axonal

direction; however, corona radiata specimens were stiffer in the direction orthogonal to the axons. Other studies reported the corona radiata to be isotropic [Shuck and Advani 1972] or have very low anisotropy [Nicolle et al. 2004] in shear. In tension, corona radiata specimens were stiffer in the axonal direction, although the results were not analyzed statistically [Velardi et al. 2006]. The inconsistency in the anisotropy of the corona radiata may be related to its fan-like structure in which there is a large spatial distribution of axonal orientation. Other studies in shear found the corpus callosum [Feng et al. 2013] and the brainstem [Ning et al. 2006] to be anisotropic with a greater stiffness in the axonal direction.

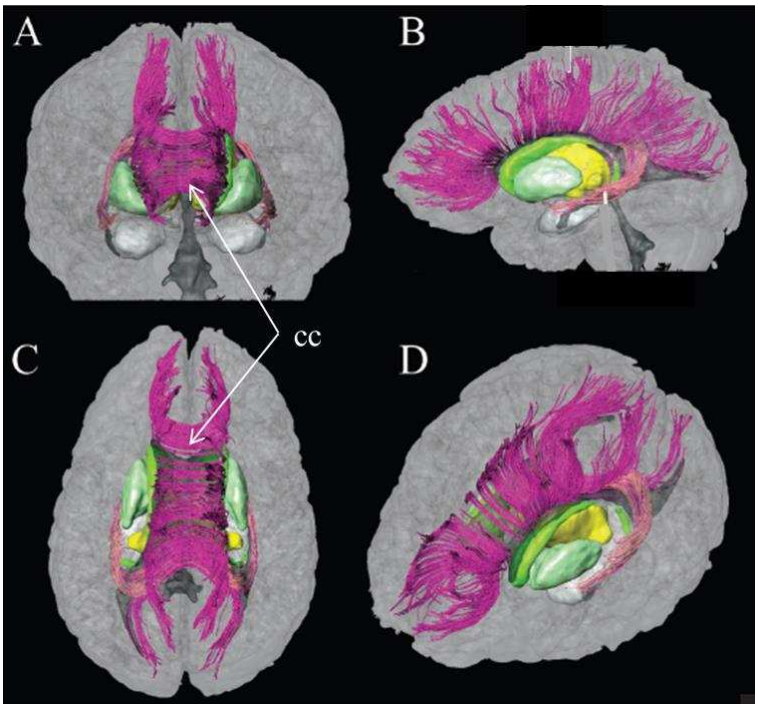

Figure 1.6: Axon tracts measured via diffusion tensor imaging are shown following outward from the corpus callosum (cc) to the cortex. The axons are highly aligned in the corpus callosum. The four views shown are (A) anterior view, (B) left lateral view, (C) superior view, and (D) oblique view from right anterior. Adapted with permission from [Wakana et al. 2004].

The data describing the anisotropy of white matter are fairly limited, with most studies only analyzing the shear behavior. The only tensile study analyzing anisotropy used specimens from the corona radiata, which has otherwise been shown to be nearly isotropic. Also, all of

these studies test the tissue in one direction at a time. However, uniaxial tests are insufficient to uniquely characterize the material [Smith and García 2013], and analyzing tissues in multi-axial loading states can more fully characterize the anisotropic behavior [Sacks 2000]. Therefore, one goal of this study is to investigate the anisotropy of white matter tissues in biaxial tension.

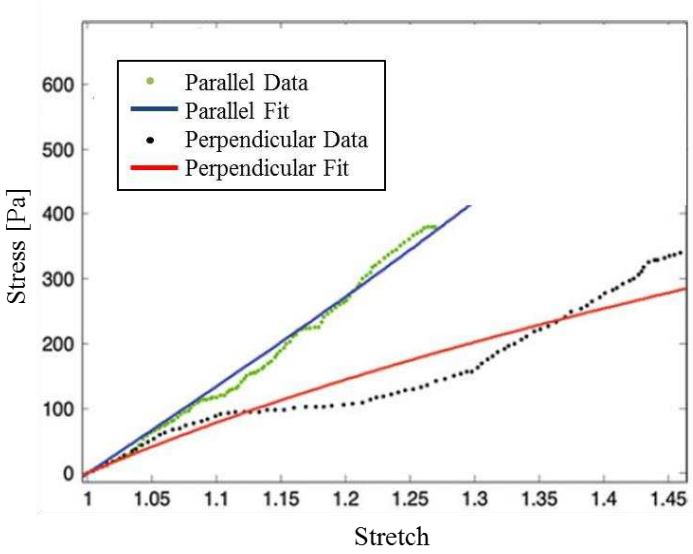

Figure 1.7: The mechanical anisotropy of white matter is shown in tension for directions parallel to and perpendicular to the axons (figure created based on published data from [Velardi et al. 2006]).

1.3.9 Preconditioning

It is typically preferred for mechanical tests on biological tissue to use a preconditioning regimen by cyclically loading the specimen until the results are unchanging between cycles (converged), and then the final loading cycle is analyzed. This process results in more reliable, less variable data [Cheng et al. 2008]. For neural tissue, however, specimens are sometimes not preconditioned due to the relatively compliant and delicate nature of the tissue [Velardi et al. 2006, Miller and Chinzei 2002, Rashid et al. 2014]. It could also be argued that it is better to assess the mechanical behavior with no prior loading history in order to more closely resemble a one-time loading event that would occur in neurosurgery. However, the brain is normally

subjected to mechanical stresses *in vivo* due to the fluctuating intracranial pressure [Steiner and Andrews 2006], as well as mechanical loads induced by accelerations of the head. Various preconditioning regimens can result in significant differences in measured material properties [Cheng et al. 2009, Gefen et al. 2003]. Based on tensile tests of spinal cords with varying preconditioning protocols, it has been recommended to precondition specimens to the highest strains that will subsequently be used in testing in order to get more repeatable results within a study and across studies [Cheng et al. 2009]. Some studies on brain tissue mechanics have chosen to precondition the specimens, and then report both preconditioned (last cycle) and non-preconditioned (first cycle) properties [Gefen et al. 2003, Gefen and Margulies 2004, Prevost et al. 2011]. When using the results of these studies, one can decide whether preconditioned or non-preconditioned properties are preferred for the specific application.

1.4 Constitutive Modeling

While many studies on brain mechanics have simplified the analysis by using the complex shear modulus to model the linear viscoelastic behavior at small strains, some attempts have been made to model the hyperelastic and nonlinear viscoelastic response of the tissue. Additional modeling approaches for soft tissues have included structural parameters into the models.

1.4.1 Hyperelasticity

Constitutive models describing hyperelasticity often take the form of strain energy density functions, which can be defined in terms the deformation gradient tensor (F), the stretches (λ_i), or a number of strain invariants. From the deformation gradient, the symmetric right Cauchy-Green strain tensor can be calculated as $C = F^T F$, and the following stain invariants can be subsequently calculated:

$$I_1 = tr(C) \tag{1.1}$$

$$I_2 = \tfrac{1}{2}[(tr\ C)^2 - tr(C^2)] \tag{1.2}$$

$$I_3 = det(C) = J^2 \tag{1.3}$$

$$I_4 = a_0 \cdot C \cdot a_0 \tag{1.4}$$

$$I_5 = a_0 \cdot C^2 \cdot a_0 \tag{1.5}$$

I_1 is related to the hydrostatic component of the deformation gradient tensor, and I_2 is related to the deviatoric strain. I_3 represents the volume change, where J is the deformed to undeformed volume ratio and equal to the determinant of F. For an incompressible material, I_3 and J are equal to unity. I_4 is an anisotropic invariant representing the square of the stretch in the direction defined by the vector a_0. I_5 is a similar invariant which can be used to describe the anisotropic shear. Defining constitutive models in terms of strain invariants offers a convenient form for computational models because they are independent of the coordinate system.

An isotropic Ogden formulation has commonly been used to model brain tissue [Miller and Chinzei 2002, Rashid et al. 2014, Franceschini et al. 2006]. The strain energy density (W) is defined as:

$$W = \frac{2\mu}{\alpha^2}(\lambda_1^\alpha + \lambda_2^\alpha + \lambda_3^\alpha - 3) \tag{1.6}$$

The coefficients μ and α represent the infinitesimal shear modulus and the stiffening (or nonlinearity), respectively. A transversely isotropic form of the Ogden model has utilized the addition of an anisotropic term to account for the axonal alignment in white matter [Meaney 2003, Velardi et al. 2006]:

$$W = \frac{2\mu}{\alpha^2}(\lambda_1^\alpha + \lambda_2^\alpha + \lambda_3^\alpha - 3) + \frac{2k\mu}{\alpha^2}\left(I_4^{\alpha/2} + 2I_4^{-\alpha/4} - 3\right) \tag{1.7}$$

In this model, the coefficient k represents the axonal component in the direction defined by I_4. Another transversely isotropic model based on a neo-Hookean solid has been used for brain tissue. A simple neo-Hookean model with an added anisotropic term was used to fit experimental shear data from the brainstem, and the model was implemented into a finite element analysis [Ning et al. 2006]. The model took the form:

$$W = C_{10}(I_1 - 3) + \frac{1}{D_1}(J-1)^2 + \frac{1}{2}\theta(I_4 - 1)^2, \tag{1.8}$$

where C_{10} is one half of the infinitesimal shear modulus, $2/D_1$ is the bulk modulus, and θ is a coefficient representing the axonal stiffness.

The coefficients for the models can be determined experimentally by fitting the experimental Cauchy stress to the theoretical Cauchy stress of the model. The theoretical Cauchy stress (σ) is derived from the strain energy density as:

$$\sigma = 2J^{-1}F \cdot \frac{\partial W}{\partial C} \cdot F^T \tag{1.9}$$

The large majority of transversely isotropic brain models have only used the I_4 invariant to model the stiffness due to the stretch in the axonal direction. Based on the anisotropic behavior of white matter in shear, it has been recommended to include contributions of the I_5 invariant [Feng et al. 2013], although the effect of an additional I_5 term has not been explored for brain tissue.

All of the models have been able to fit stress-strain data well; however, model assessment should also assess their predictive power. One study used three different formulations (a Fung model, a Gent model, and an Ogden model) to model tensile and compressive data separately, and all three models fit the data equally well [Rashid et al. 2012, Rashid et al. 2014]. However, because the model fits to tension and compression were done separately, the study did not assess the robustness or predictive ability of the models when applied to independent data. However,

an Ogden model fitted to shear data has been able to predict the compressive behavior in an independent experiment [Prange and Margulies 2002].

Most of the brain constitutive models assume the tissue to be incompressible. A term including I_3 or J, as in equation (1.8), can be used to model the volume change for a compressible material. By including the volume change in one model, compressible and incompressible models of brain tissue have been found to be indistinguishable [Laksari et al. 2012], agreeing with previous work showing brain tissue to be nearly incompressible [Holbourn 1943].

1.4.2 Inclusion of structural parameters into models

Microstructural approaches have been used to describe the specific mechanics of axon and matrix components. Similar to fiber crimp in collagenous tissues, axonal undulation has been observed in the guinea pig optic nerve via neurofilament staining [Bain et al. 2003]. The recruitment of the axons while stretching was modeled to describe the gradual coupling of the axons to the glial cells. This study provided evidence for non-affine mechanics of the axons and glial matrix at low stretches, transitioning to increased affinity at higher stretches. In affine mechanics, the structural components (axons) and bulk material (matrix) are coupled and experience the same deformations, but in non-affine mechanics, the structural components can deform separately from the bulk material. A non-affine model has been incorporated into finite element analyses that treat the axons and matrix as separate materials, reporting the relative stresses in each material [Karami et al. 2009, Pan et al. 2011]. It was found that greater undulation resulted in relatively higher matrix stresses and lower axonal stresses [Karami et al. 2009]. When comparing this structural constitutive model to phenomenological hyperelastic models, it was found that the Ogden and Fung hyperelastic models could match the overall

behavior of the structural model, but a Mooney-Rivlin model resulted in higher errors [Meaney 2003]. While the undulation microstructural model can be useful for modeling the specific mechanical response of axons and the glial matrix, hyperelastic models are sufficient for modeling the tissue-level response.

Another structural modeling approach involves the measurement of axon volume fraction. One group used volume fraction measurements to determine the difference between axon and matrix properties. They estimated the complex shear modulus for axons and matrix separately via shear experiments on the optic nerve and brainstem [Abrogast and Margulies 1999]. The axonal moduli were estimated from the optic nerve because it contains a high volume fraction of axons (>90%), and the brainstem was taken as an axon-matrix composite to estimate the matrix moduli. The brainstem contains a structure of bundled axons, and the volume fraction was measured via histology with stained white matter and unstained grey matter. In the brainstem, the axons had a volume fraction of 0.53±0.07, and were about three times stiffer than the matrix [Abrogast and Margulies 1999]. While this study estimated volume fraction of axons from the area of stained white matter, similar measurements have been made using transmission electron microscopy, giving the ability to visualize individual axons [Kim et al. 1996]. An axon-matrix composite finite element approach found that increasing the volume fraction of axons increased the resulting stresses, with a greater effect at higher strains [Karami et al. 2009]. While this approach defined two separate materials to give the difference between axons and matrix, a single constitutive model could be used to describe white matter as a whole, and incorporate the axon volume fraction as a parameter in the axonal term of the model.

Fiber dispersion has been incorporated as a parameter in constitutive models of soft tissues. A parameter defining the statistical distribution of collagen fiber orientation has been

incorporated into a Holzapfel hyperelastic model of blood vessel walls [Gasser et al. 2006]. This parameter affects the degree of anisotropy in the fiber response. However, the dispersion parameter was estimated via model fits rather than empirically measured. A similar modeling approach has been used, with the exception that the distribution was experimentally derived. This model was able to fit biaxial tests of pericardium [Sacks 2003]. Measures of dispersion have not been incorporated into brain constitutive models even though some regions of the brain such as the corona radiata show a high spatial distribution of axons (Figure 1.8).

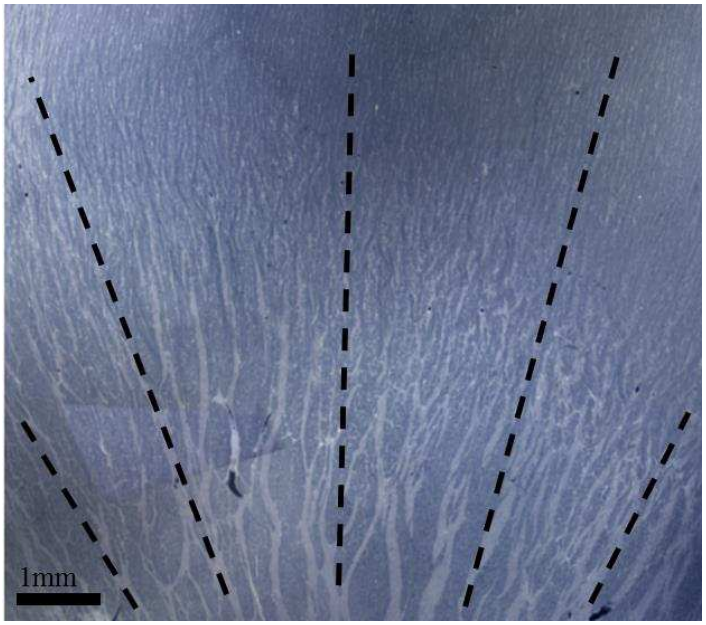

Figure 1.8: Histology section of ovine corona radiata stained for myelin with Luxol Fast Blue, with the spatial distribution of the axonal orientation marked with dashed lines.

One goal of the current study is to incorporate empirical measurements of axon volume fraction and distribution into a constitutive model describing the results from white matter mechanical testing.

1.4.3 Viscoelasticity

Like most soft tissues, brain tissue is a viscoelastic material. Because surgical operations are dynamic (although low-speed) events, it is important for surgical simulations to model the

viscoelastic behavior of brain tissue [Kyriacou et al. 2002]. Viscoelastic models can be generally be divided into three categories: linear, quasi-linear, and fully nonlinear viscoelastic formulations.

Under the assumption of linear viscoelasticity, the constitutive model for the stress (σ) can be given as:

$$\sigma(t) = \int_0^t E(t-\tau)\frac{\partial \varepsilon(\tau)}{\partial \tau} d\tau, \tag{1.10}$$

where *E(t)* is the relaxation modulus, *ε(t)* is the strain, and τ is a time variable of integration. If equation (1.10) is applied to cyclic strains, the stress can then be given in terms of a complex modulus:

$$\sigma(t) = (E' + iE'')\varepsilon(t) \tag{1.11}$$

where E' and E'' are the storage and loss moduli, respectively. Many studies have done frequency sweep experiments for oscillatory shear, covering high strain rates. They are often done at low strains, assuming linear viscoelasticity [Hrapko et al. 2008], and the reported complex moduli are commonly implemented in computational models [Post et al. 2012, Zhang et al. 2001]. However, linear viscoelastic models of brain tissue are only valid at low strains (less than 0.01) [Nicolle et al. 2004]. Since the surgical operations involve larger strains [Garcia et al. 2012], it is suggested that nonlinear viscoelastic models should be used to accordingly predict the internal tissue mechanics.

The Fung model of quasi-linear viscoelasticity is commonly used to model soft tissues [Fung 1993]. In this model, the stress is expressed as a function of stretch (λ) and time (t), at an instance of time τ, using a single hereditary integral:

$$\sigma(t) = \int_{-\infty}^t G(t-\tau)\frac{\partial \sigma^{(e)}[\lambda(\tau)]}{\partial \lambda}\frac{\partial \lambda(\tau)}{\partial \tau} d\tau \tag{1.12}$$

$\sigma^{(e)}$ is the instantaneous elastic response, and is typically approximated by the stress response at a high loading rate. When applied to brain tensile stress-relaxation experiments, the elastic response has taken the form of an Ogden hyperelastic model (equation 1.6) [Rashid et al. 2014]. The reduced relaxation function *G(t)* is normalized such that *G*(0) = 1. This function is often simplified to be represented by a Prony series:

$$G(t) = 1 - \sum_{i=1}^{n} C_i(1 - e^{-t/\tau_i}) \tag{1.13}$$

where τ_i are relaxation time constants, and C_i are the corresponding coefficients. In this formulation, the elastic response can be nonlinear, but the relaxation function does not take into account nonlinearities in the relaxation with respect to strain magnitude. A fully nonlinear viscoelastic model can better represent the nonlinearities in both the stress-strain relationship and in the relaxation behavior with respect to strain magnitude.

One approach to modeling nonlinear viscoelasticity, which has been applied to spinal cord tension [Shetye et al. 2014], defines the relaxation modulus in equation (1.10) as a function of time and strain, such that

$$E(t, \varepsilon) = E_\infty(\varepsilon) + \sum_{i=1}^{4} E_i(\varepsilon) e^{-t/\tau_i}\ , \tag{1.14}$$

where E_∞ represents the long term steady state modulus, and the E_i moduli correspond to the time constants. *E(ε)* can be defined as a quadratic function with coefficients C_1 and C_2:

$$E(\varepsilon) = C_1\varepsilon + C_2\varepsilon^2. \tag{1.15}$$

This model uses a ramp correction method to account for finite ramp times in stress-relaxation experiments [Troyer et al. 2012a], and was able to represent the spinal cord ramp response [Shetye et al. 2014]. The experimental cyclic response of the spinal cord could also be predicted. The model has effectively been implemented into a finite element analysis [Troyer et al. 2012b].

The viscoelastic models of brain tissue have rarely considered the anisotropy of white matter, and those that do account for directionally-dependent behavior have exclusively used linear viscoelasticity [Abrogast and Margulies 1999, Feng et al. 2013, Nicolle et al. 2004]. However, anisotropic nonlinear viscoelastic models have been formulated for other soft tissues [Bischoff et al. 2004, Nguyen et al. 2008]. Anisotropic viscoelastic behavior can be modeled in multi-dimensional loading states, such as biaxial stress, by modifying equation (1.12) [Fung 1993]. $\sigma(t)$, $G(t)$, and $\sigma^{(e)}(\lambda)$ are replaced with the tensors $S_{ij}(t)$, $G_{ijkl}(t)$, and $S_{kl}^{(e)}(E)$, respectively, where S is the 2nd Piola-Kirchhoff stress and E is the Green-Lagrange strain tensor, resulting in:

$$S_{ij}(t) = \int_{-\infty}^{t} G_{ijkl}(t-\tau) \frac{\partial S_{kl}^{(e)}[E(\tau)]}{\partial E} \frac{\partial E(\tau)}{\partial \tau} d\tau \tag{1.16}$$

In the case of biaxial tension with negligible shear, there are three independent relaxation functions: G_{1111}, G_{2222}, and G_{1122}. These relaxation functions have been used to analyze the stress relaxation in longitudinal and circumferential directions in a urinary bladder biaxial test [Nagatomi et al. 2004]. This approach allows for a determination of the anisotropy of the relaxation behavior separately from the anisotropy of the elastic behavior, and could be applied to model the anisotropic viscoelastic behavior of brain white matter in biaxial tension.

1.5 Probabilistic Analysis

In biomechanics, computational modeling is used to make predictions about a system response, which can be the motion of a joint, localized stresses and strains, or some structural failure. Models are often based on a single geometry with material properties taken from experimental means. However, in biological system data there are high variability in material properties and geometries. Probabilistic modeling approaches have taken the variability into account to predict the probability distribution of a response based on the distributions of the input parameters (material properties, geometries, etc.). For example, a finite element model was

used to assess the effects of the variability of ligament stiffness, attachment point, and reference strain on the kinematic constraint on the knee joint [Baldwin et al. 2009]. Importance factors were calculated to determine the relative specificity of ligament properties on the joint constraint. As another example, a femur finite element model utilized the variability in bone stiffness and strength relative to predicted properties derived from computed tomography scans [Keller 1994]. The model predictions of fracture risk found that the 1-99% probability range of risk was greater than 50% of the mean risk [Laz et al. 2007].

In the brain, a probabilistic modeling approach could be used to predict the probability distribution of model stress and strain predictions. The stress and strain response in the model would be influenced, in part, by the distribution of the material parameters. One goal of this study is to report the distribution of constitutive model parameters fitted to biaxial experimental data, and to use this distribution to predict the distribution of the stress response.

Probabilistic methods start with the distribution of input parameters, which can be defined by a number of statistical distributions (normal, lognormal, etc.). Combinations of the input parameters are then sampled based on their distributions, and a model is used to predict the output response. With enough sampling, the full probability distribution of the response can be calculated. The Monte Carlo method of sampling is the gold standard probabilistic method. It uses random sampling of the input parameters according to their distribution. It is simple and robust, but requires thousands of trials in order to guarantee accuracy. Other methods are able to achieve similar accuracy while using far fewer trials, which is advantageous if computational cost is a concern. One common method is the advanced mean-value method which, in short, uses a mean-based response to determine the most probable point for the model performance for a given probability level [NESSUS Theoretical Manual]. The number of trials needed depends

on the number of input parameters and the number of desired probability levels. It is recommended to validate the use of the advanced mean-value method (or any other approximation method) against the Monte Carlo method for any new model [Laz and Browne 2010]. The advanced mean-value method has accurately matched the Monte Carlo method in previous probabilistic models, while reducing the computational time up to 400 fold [Baldwin et al. 2009, Laz et al. 2007].

In addition to giving the probability distribution of the model response, probabilistic methods can provide information about the sensitivity of the model to the input parameters. Correlations are a starting point to determine the relations between parameters. Probabilistic methods allow the computing of absolute sensitivity factors, defined as the derivative of the model response probability with respect to the mean and standard deviation of the input parameters, normalized by the standard deviation and probability [NESSUS User Manual]. Importance factors can also be calculated to provide the relative importance of the parameters to the probability of the model response.

1.6 Summary

The overarching goal of this study was to improve the anisotropic mechanical behavior descriptions of brain tissue in computational models used for simulated neurosurgery.

Finite element models of the brain require accurate material models. Brain tissue exhibits hyperelastic and viscoelastic qualities, with white matter being anisotropic and grey matter being isotropic. This behavior has been determined through experiments in compression, shear, and tension, and described using continuum models. However, there is a lack of data describing the effects of multi-axial loading, even though *in vivo* brain tissue is in a constant multi-axial stress state due to fluid pressure. Data from uniaxial experiments do not sufficiently describe

simultaneously applied multi-axial stresses. Therefore, biaxial tensile experiments were developed to more fully characterize the anisotropic behavior of white matter in quasi-static and dynamic loading states, and elucidate any interaction effects arising from a biaxial state of stress.

Many studies derive material definitions from a mean behavior of tissues assumed to be homogeneous. However, the properties of white matter have been shown to be regionally dependent. Also, axonal orientation can be heterogeneous in certain regions of the brain, and the resulting anisotropy can have substantial effects on brain finite element model predictions. Moreover, there is a lack of information relating the mechanical behavior of a given specimen to its specific structural properties. Linking the mechanical behavior of white matter to the orientation, spatial distribution, and volume fraction of axons can provide important insight with respect to the structure-function relationship of the tissue and allow for more accurate material models and computational predictions. The mechanical data of brain tissue exhibit a high degree of variability. Probabilistic analyses can be utilized to quantify the uncertainty in model predictions arising from input parameter variability.

The purpose of this study was to use a combined experimental and computational approach to describe the biaxial mechanics of brain white matter in both static and dynamic loading scenarios, and to gain a deeper understanding of the relationship between brain tissue structure and mechanical behavior.

1.7 Specific Aims

In order to achieve the aforementioned goals, we have proposed the following specific aims:

Specific Aim 1: Perform quasi-static biaxial experiments in order to describe the anisotropic material behavior of brain white matter.

A procedure was developed to test the biaxial mechanics of white matter under quasi-static loading in order to establish an anisotropic hyperelastic model formulation. Experiments were performed on fresh ovine brain white matter from two regions: the corona radiata and the corpus callosum. The testing protocol utilized three biaxial displacement ratios as well as uniaxial loading tests in both directions. An anisotropic Ogden constitutive model was fitted to the experimental data. The results were the first to characterize the biaxial mechanical behavior of brain tissue, which can contribute to elevating the accuracy of computational models.

Specific Aim 2: Model the biaxial experiments using an anisotropic continuum model that incorporates measured structural parameters.

The mechanical behavior of each specimen from the biaxial experiments were related to structural parameters measured via imaging analyses. The following imaging analyses were performed:

- Histology was performed to define axon orientation and distribution.
- Transmission electron microscopy was used to measure axon volume fraction.

In order to test a variety of structural properties, specimens were used from two anatomic locations: the highly aligned corpus callosum and the more disperse corona radiata. The measured structural parameters were incorporated into the anisotropic axonal term of the constitutive model. The model was analyzed using a probabilistic (i.e. stochastic) approach to quantify uncertainty in the stress predictions due to variability in the model parameters. It was hypothesized that the inclusion of measured structural parameters into the model would decrease the variability of the model predictions. This would allow for greater certainty in the predictions made from computational models.

Specific Aim 3: Model the anisotropic nonlinear viscoelastic properties of white matter via biaxial stress-relaxation and cyclic loading experiments.

Because brain tissue exhibits viscoelastic properties, characterizing the quasi-static behavior does not provide enough information for accurate models. The developed biaxial test was extended to characterize the anisotropic viscoelastic properties of white matter. The biaxial testing setup developed in Specific Aim 1 was used to perform biaxial stress-relaxation and cyclic loading experiments. In order to determine the nonlinear (strain-dependent) viscoelastic properties, the experiments utilized a variety of equibiaxial strain magnitudes. The biaxial tests also allowed for the anisotropy of the time-dependent behavior to be determined separately from the elastic behavior. An anisotropic viscoelastic constitutive model was fitted to the stress-relaxation experiments, and the model was assessed via predictions of cyclic experiments. Additionally, the distribution of the model parameters was determined and used to find the probability distribution of model stress predictions and the sensitivity of the model to the variance of the input parameters.

2. AN ANISOTRPIC HYPERELASTIC CONSTITUTIVE MODEL OF BRAIN WHITE MATTER IN BIAXIAL TENSION AND STRUCTURAL-MECHANICAL RELATIONSHIPS[1]

2.1 Introduction

Accurate characterization of the mechanical behavior of brain tissue is required for computational models used for simulated neurosurgery. These models are useful for surgeon training, operation planning, and image registration to account for intraoperative brain shifts [Ferrant et al. 2001, Miller 2011]. Examples of surgical procedures include craniotomies, tumor debulking, and injections for drug delivery [Chan et al. 2013, García et al. 2012]. Computational models require accurate constitutive descriptions of the stress-strain relationship to compute the finite deformations that occur during exogenous loading and surgical procedures.

White matter is structurally anisotropic due to the alignment of axon tracts connecting various regions of the brain. White matter has also been shown to be mechanically anisotropic via *in vitro* experiments in uniaxial tension, shear, compression, and indentation [Feng et al. 2013, Ning et al. 2006, Prange and Margulies 2002, Velardi et al. 2006]. This mechanical behavior has been modeled using transversely isotropic hyperelastic continuum models that contain an isotropic term to describe the glial matrix and an anisotropic term to describe the axonal contribution [Feng et al. 2013, Ning et al. 2006, Velardi et al. 2006]. Each of these experiments have demonstrated anisotropy by testing the tissue in directions parallel and perpendicular to the axons, with the axonal direction being stiffer in tension and shear than the transverse direction. However, the aforementioned mechanical characterization of white matter

[1] *This chapter is in press for publication as a Research Article in the Journal of the Mechanical Behavior of Biomedical Materials (doi:10.1016/j.jmbbm.2016.05.003). The text and figures have been adapted from Elsevier.*

was limited to testing in one direction at a time, and uniaxial testing is insufficient to uniquely characterize the material [Smith and García 2013]. Accordingly, there is no information on the mechanical behavior during simultaneous multi-axial loading. The behavior in a multi-axial loading state may differ due to structural interactions between the axons and interconnected glial cells [Shreiber et al. 2009]. The multi-axial mechanics of the brain are relevant due to the intracranial pressure and the complex loading that is typically experienced during surgical procedures. Biaxial tensile tests can be used to better determine any multi-axial mechanical interactions that are present and better simulate the inherently constrained loading to which the brain is subjected to *in vivo*.

Computational models of the brain are typically based on a single geometry with material properties derived from experimental cohorts. However, these models lack information on the variability of the specimen population and usually adopt mean values. Probabilistic modeling approaches take into account the variability of input parameters (geometry, material properties, etc.) to predict the probability distribution of a model response instead of relying on the mean response [Laz and Browne 2010]. In studies of the brain, this approach would be useful for providing a measure of uncertainty in surgical simulations or for predicting the probability of an event such as an injury [Bain and Meaney 2000]. It is therefore advantageous to provide probability distributions in the derivation of material constitutive models and to use accurate models to minimize uncertainty in their resultant predictions.

Many studies derive material definitions from a mean behavior of tissues assumed to be homogeneous. However, the properties of white matter have been shown to be regionally dependent [Prange and Margulies 2002, Velardi et al. 2006]. Axon orientation can be heterogeneous in certain regions of the brain, and the resulting anisotropy can have substantial

effects on brain finite element model predictions [Colgan et al. 2010, Wright and Ramesh 2012]. Some promising modeling approaches for biological tissues have incorporated a fiber dispersion parameter into constitutive models [Gasser et al. 2006, Sacks 2003], while other research groups have used axon volume fraction measurements in a composite modeling approach of brain tissue [Abrogast and Margulies 1999, Karami et al. 2009]. However, there is a lack of information relating the mechanical behavior of a given specimen of brain tissue to its specific structural properties. Linking the mechanical behavior of white matter to the structural properties of axons may provide important insight with respect to the structure-function relationship of the tissue and allow for more accurate material models and computational predictions.

The purpose of this study was to develop a robust testing procedure to perform a biaxial test of brain white matter and to model the mechanical behavior using an anisotropic hyperelastic continuum model. In order to achieve this aim, we related the axon orientation, distribution, and volume fraction to the mechanical behavior of white matter specimens. These measured properties were implemented into a structurally-based constitutive model, and a probabilistic analysis was used to determine if the structural model decreases uncertainty in the model stress predictions compared to a standard hyperelastic model.

2.2 Methods

Biaxial tensile experiments were performed on white matter from the corona radiata and corpus callosum of ovine brains. Histology and transmission electron microscopy were used to make image-based measurements of structural properties of the axons. Biaxial experiments were fitted to anisotropic hyperelastic constitutive models with and without the implementation of measured structural properties.

2.2.1 Parametric series and pilot studies on biaxial geometry effects

A preliminary finite element study investigated the effects of specimen geometry on the degree of homogeneity of the central region strain field for clamped specimens. Models were created using ABAQUS (ver. 6.11, Simulia, Providence, RI) for four geometries: square, cruciform, cruciform with rounded corners, and octagon. Since the purpose of the preliminary study was to guide the selection of specimen geometry and not to investigate the effects of material properties, a simple linear elastic model was used with an elastic modulus of 3200 Pa, and Poisson's ratio of 0.499 [Miller et al. 2000]. Identical displacement boundary conditions were applied to each model in a 1:1 displacement ratio. A 2 mm displacement applied in each direction corresponded to an 8% global strain. Strains were analyzed in a central 5mm square region of interest by measuring the homogeneity of the strain field and the shear strain.

For all four model geometries, the longitudinal strain at the center node was consistent, ranging from 6.18% to 6.43%. The cruciform geometry resulted in the most homogeneous strain field within the region of interest, with a range of strains of only 0.29%. The cruciform also demonstrated the lowest shear strain (0.86%) within the region of interest. Although the material model was simplified, this preliminary study directly compared biaxial geometries. A more extensive study similarly showed lower stress concentrations and improved load transfer to the region of interest for a cruciform shape as compared to a perfectly square geometry [Jacobs et al. 2013]. This result was found to be the case for both isotropic and transversely isotropic models.

In a separate finite element study, the thickness of the model was varied to analyze the effects, if any, of the specimen's aspect ratio. While it is ideal to have very thin specimens (high aspect ratio) in order to satisfy the plane-stress assumption in a biaxial analysis, it is also necessary to have a specimen thickness that allows for consistent dissection of the very soft

tissue. In this study, the thickness was varied on the cruciform model to produce aspect ratios of 2:1, 3:1, 5:1, 10:1, and 50:1, and these model variants were compared to a two-dimensional plane-stress model. The same 2 mm displacement loading conditions were applied, and the out-of-plane and longitudinal stresses were measured at the center of each model.

It was found that the maximum out-of-plane stress and the percent difference in longitudinal stress from the plane-stress model both decreased and approached zero with increasing aspect ratio. An aspect ratio of 3:1 was determined to sufficiently satisfy the plane-stress assumption because the percent difference in longitudinal stress was less than 1%. Additionally, the out-of-plane stress was 3.9 Pa, compared to 200 Pa in the longitudinal direction.

Based on the results of these pilot studies, the biaxial experiments were conducted using a cruciform shaped specimen with an aspect ratio of 3:1. The cruciform shape demonstrated the most homogeneous region of interest and lowest shear, and the 3:1 aspect ratio sufficiently satisfied the plane-stress assumption.

2.2.2 Dissection

Ovine brain tissue specimens were dissected immediately (less than one hour) after animals were euthanized for unrelated studies. Testing was performed on white matter specimens from two regions of the brain: the corona radiata and the corpus callosum (n = 9 samples for each region). Axons in the corona radiata extend radially outward from the globus pallidus to the cerebral cortex in both hemispheres of the brain. Corona radiata specimens were dissected by removing a slice from one brain hemisphere in the sagittal plane, halfway between the mid-sagittal plane and the outer edge of the brain, using a custom drop slicer with two blades spaced 2 mm apart (Figure 2.1). From this slice, a cruciform shape was punched such that the

central square contained only white matter between the globus pallidus and the cerebral cortex. The corpus callosum is a wide thin structure located centrally in the brain and connects the two hemispheres. The corpus callosum was isolated from an intact brain, and slices were cut using a scalpel to separate the corpus callosum from the adjacent grey matter. A cruciform shape was punched from one lateral side such that the central square of the specimen did not include the midline bifurcation, where the septum pellucidum meets the corpus callosum, in order to avoid an inhomogeneous structure in the region of interest. Specimen shapes were punched such that the dominant axonal direction was visually coincident with one of the loading directions. The actual orientation was determined via *post hoc* measurements from histology sections.

After isolating slices, but prior to punching the cruciform shape, each slice was placed on a plate and submerged in saline. The low friction environment allowed the slice of tissue to return to a state of equilibrium stress, minimizing residual stresses that were induced by handling of the tissue. While it has been reported that residual stresses can alter the in vivo mechanical environment of the brain [Xu et al. 2009], we did not observe any gross deformations after cutting the cruciform shape.

In order to perform *post hoc* calculations of the imposed stress, the cross sectional area of specimens was determined. Specimen thickness was determined via electrical connectivity measurements in which the specimen was placed on a conducting plate, which was connected to one lead of a voltmeter. The other lead was attached to a fixed caliber and lowered to the top surface of the specimen until contact was achieved, as detected by a change in voltage (Figure 2.1).

The specimen's width and length were measured optically by imaging the specimen with a ruled scale, and measuring the dimensions using ImageJ. The mean thickness was 1.9 mm, and

the mean width was 7.0 mm. Pilot studies on larger specimens (12mm x 4mm) had resulted in heterogeneous specimens that included some grey matter as well as a highly variable distribution of axon orientation. Therefore, the specimen size was reduced by approximately 50% in each dimension. Extreme care was taken throughout the dissection process so as not to stretch the very soft, easily damaged tissue. Specimens were kept hydrated with periodic saline spray. All testing was completed within six hours post-mortem in order to minimize any changes due to tissue degradation [Garo et al. 2007].

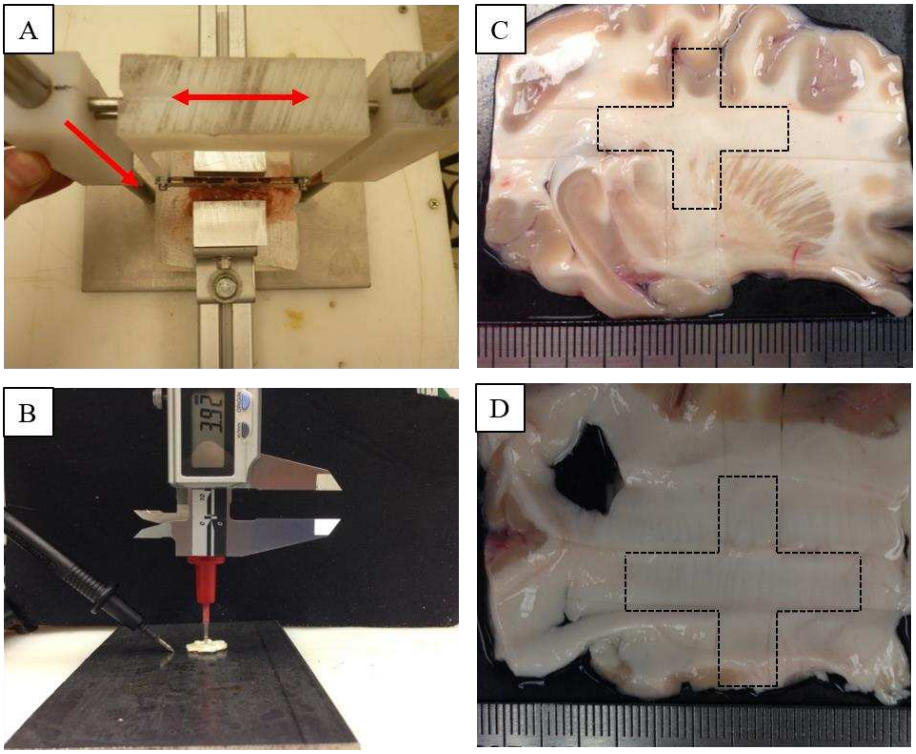

Figure 2.1: (A) A custom slicer was used to cut specimens of uniform thickness. Red lines indicate freedom of movement for manual slicing. (B) Thickness was measured via electrical connectivity. Cruciform specimens were dissected from either (C) the corona radiata from slices in the sagittal plane, or (D) the corpus callosum from slices in the transverse (horizontal) plane.

2.2.3 Testing Setup

In order to obtain a true state of biaxial tension and minimize shear, all four specimen grips must be unrestricted for lateral movement while the specimen is being tensioned. In a

biaxial test of biological tissue, this is usually accomplished by gripping the specimen with sutures, and the wire is free to rotate around a pivoting point. However, brain tissue is too soft to grip with sutures without tearing. Also, it was found that the weight of the brain specimen, when suspended from wires, was sufficient to produce a pre-tension that is higher than desired. In order to allow for free lateral movement without suspending the specimen, foam grips were designed to float the specimen on the surface of a saline bath. Each specimen was attached to four floating grips via a cyanoacrylate adhesive (Figure 2.2). Each grip was then attached to the biaxial testing apparatus via a wire that was of sufficient length such that unrestricted rotations of the wire about a pivoting point resulted in lateral movement of the grips. Two of the grips were attached to linear actuators (T-LLS, Zaber Technologies Inc., Vancouver, BC, Canada), and the remaining two grips were attached to 250 gram capacity load cells (Model 31, Honeywell Sensotec, Columbus, OH). The saline bath ensured that the specimen remained hydrated throughout the test.

2.2.4 Experiments

Specimens were initially loaded to a preload of 1.0 mN (mean stress of 71 Pa). This was followed by an initial preconditioning regimen of five cycles at a 1:1 (axonal: transverse) displacement ratio, which stretched the specimen to the highest stretch levels experienced throughout testing in order to have a reproducible loading history [Cheng et al. 2009]. After 10 minutes of recovery time, the experiment consisted of three biaxial tests at 1:1, 1:0.5, and 0.5:1 displacement ratios, and two uniaxial tests, all in a randomized order. For the uniaxial tests, the grip attachments (i.e. constraints) were removed in the non-tested direction. The maximum displacement for each test was 3mm, which corresponded to a mean stretch of 1.15. Each test was performed for five cycles at a rate of 0.05 mm/s in the direction of greater stretch (mean

strain rate of 0.0025 s^{-1}), and the specimen was allowed to recover for 10 minutes between each test.

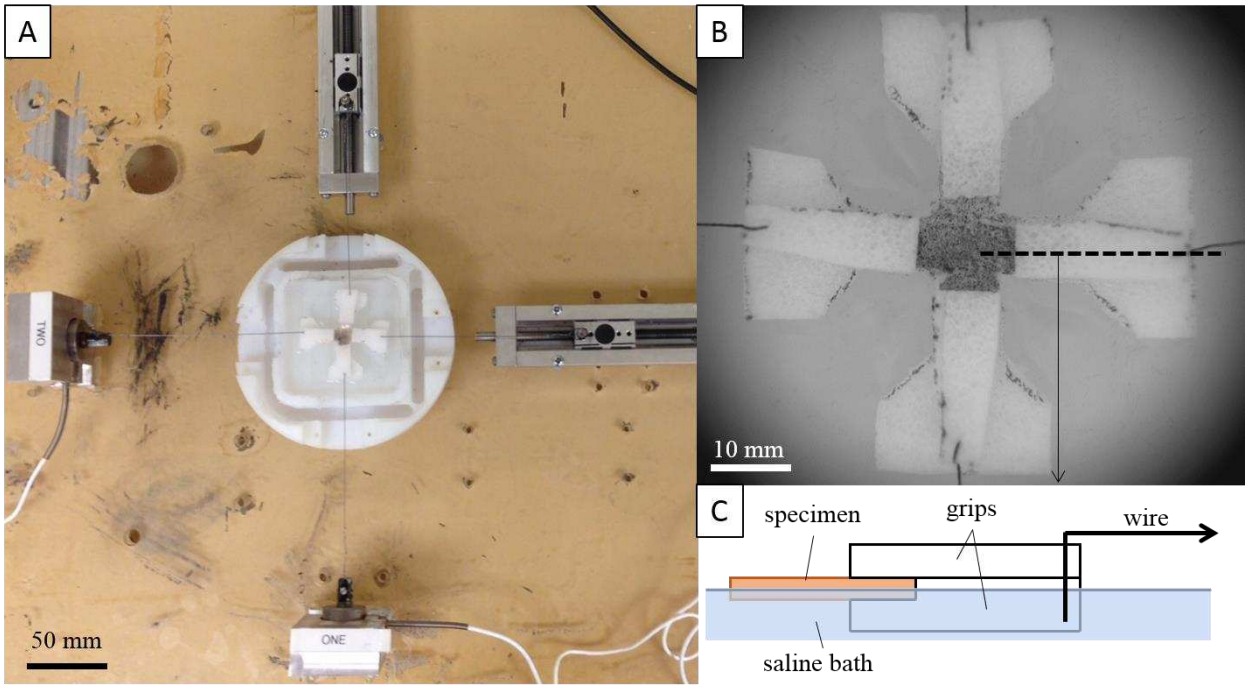

Figure 2.2: (A) Biaxial testing setup showing specimen floating on saline bath and connected to two load cells and two linear actuators. (B) The grip design is shown, along with the side view (C).

In order to track the deformations, graphite powder was dusted on the top surface of the specimens, and images were recorded throughout each test. Stretches were calculated via a MATLAB-based digital image correlation program. The digital image correlation was used to create strain maps of the entire specimen area, as well as calculate average stretch values in the region of interest, which was defined as a 15x15 mesh, creating a 2.4 mm square in the center of the specimen. Image resolution was determined to be 32 μm/pixel

2.2.5 Structural Analysis

Post hoc structural imaging analyses were performed on the specimens used for the biaxial experiments. Histology was performed on planar sections in order to measure two

structural parameters: mean axonal orientation (θ_m) and axonal distribution (κ). Transmission electron microscopy (TEM) was performed on cross-sectional cuts in order to obtain the resolution necessary to image individual axons and measure the axonal volume fraction (f_a) [Kim et al. 1996]. In order to get planar sections for histology and cross-sections for electron microscopy, each cruciform specimen was cut at the base of the two arms which extended in the axonal direction. For each of the two arms, electron microscopy sections were taken in the plane of the cross-sectional cut. The remaining central square was processed for histology and sectioned in the plane of testing.

2.2.6 Histology

Immediately after mechanical testing, cut specimens were stored in 10% buffered formalin phosphate solution for at least two weeks. Specimens were dehydrated using a series of ethanol washes, embedded in paraffin wax, and cut to 10 μm thick sections using a microtome. All sections were cut in the plane of testing, and five slides were produced per specimen, with sections taken throughout the thickness. Slides were deparaffinized and stained for myelin using Luxol Fast Blue.

Transmitted light microscopy images were analyzed using a custom MATLAB program that overlaid a 6x6 grid of lines onto the same central region of interest that was used for the biaxial strain measurements. Each line was aligned with the local axonal orientation (Figure 2.3). The mean orientation (θ_m) was calculated as the arithmetic average angle of the lines relative to the axis of loading that had been visually aligned with the axons upon dissection. Since the direction of the angle is irrelevant to the modeling, θ_m was defined as the absolute value of the mean angle.

The axonal distribution parameter (κ) was originally derived to describe the distribution of collagen fibers in arterial walls [Gasser et al. 2006]. The parameter is defined as:

$$\kappa = \frac{1}{4}\int_0^{\pi} \rho(\theta) sin^3(\theta) d\theta \tag{2.1}$$

where θ is a random variable defining the fiber angle, and $\rho(\theta)$ is a normalized fiber angle density function of the form:

$$\int_0^{\pi} \rho(\theta) sin(\theta) d\theta = 2 \tag{2.2}$$

κ can range between 0 and 1/3, with κ = 0 representing perfectly aligned axons and κ = 1/3 representing randomly aligned axons resulting in an isotropic material. Equations (2.1) and (2.2) were used to calculate κ from the distribution of orientations of the grid points overlaid on the specimen images. Means were calculated from the five sections per specimen.

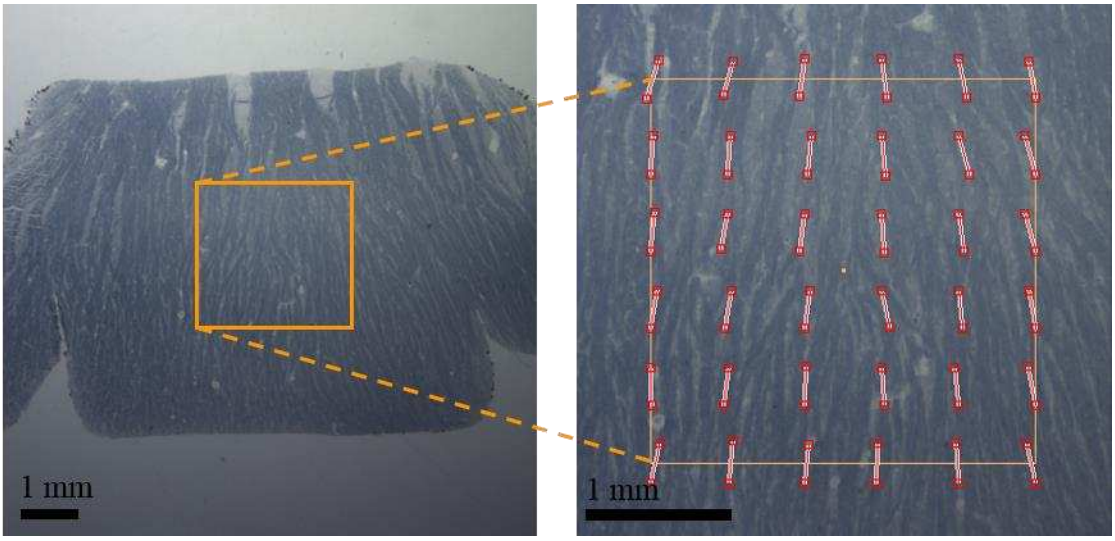

Figure 2.3: Image of biaxial specimen showing the grid used for measuring mean axon orientation and distribution. The lines overlaid on the right image were manipulated by the user to be aligned with the local orientation of the axons. The angle of each line relative to the specimen orientation was measured and used to calculate θ_m and κ.

2.2.7 Transmission Electron Microscopy

Immediately after testing, the specimen arms in the axonal direction were fixed in a 2% glutaraldehyde, 2% paraformaldehyde phosphate buffer solution overnight. After fixation, the

specimens were washed with phosphate buffer and cut to six 1mm blocks per specimen (three blocks per arm). The blocks were stained with 2% osmium tetroxide for one hour, dehydrated through a series of ethanol washes, and embedded in an epoxy resin. Blocks were sectioned to 90nm using an ultramicrotome, mounted to grids, and stained with uranyl acetate and lead citrate. The sections were imaged at 15,000X magnification using a transmission electron microscope (JEOL 1400, JEOL USA Inc., Peabody, MA). Three images were taken at random locations from each of the six blocks to get 18 total images per specimen.

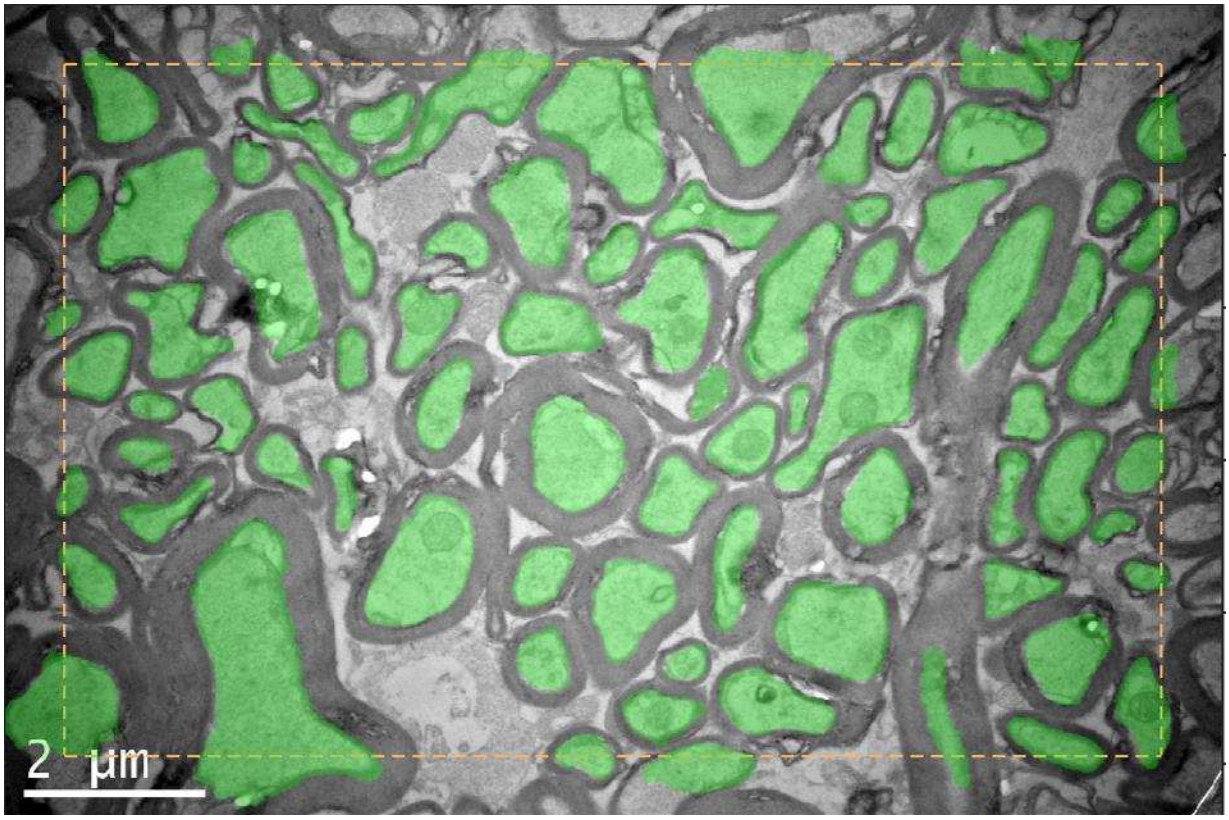

Figure 2.4: Segmented TEM image of a corpus callosum specimen. The segmented axons are shaded green, and the measurements were only taken within the dotted-line rectangle.

Axon volume fraction measurements were made by manually segmenting the axons in the image using a custom MATLAB segmentation program and measuring the area fraction (Figure 2.4). The volume fraction was taken as the mean measurement from the 18 images.

Myelinated axons were abundant and could easily be distinguished by the dark layered rings of myelin surrounding the axons. Unmyelinated axons were uncommon but could be distinguished from glial cells by their round shape and the presence of microtubules. On the other hand, oligodendrocytes were larger, irregularly shaped, and had a dark-stained nucleus and cytoplasm. Astrocytes were also larger and irregularly shaped, but with a light colored cytoplasm.

2.2.8 Modeling

Two modeling approaches were used to represent the mechanical data. The first "basic" model was an anisotropic form of an Ogden hyperelastic strain energy density function, and the second "structural" model incorporated the measured structural parameters into the same function. Both models were formulated as functions of the principal stretches, λ_i. With shear strains assumed to be negligible, the three-dimensional deformation gradient tensor, F, can be simplified as:

$$F = \begin{bmatrix} \lambda_1 & 0 & 0 \\ 0 & \lambda_2 & 0 \\ 0 & 0 & \lambda_3 \end{bmatrix}, \tag{2.3}$$

where λ_1 and λ_2 are the measured stretches in the two tested directions, and λ_3 is the stretch in the out-of-plane direction. The tissue was assumed to be incompressible; therefore λ_3 can be found by:

$$\lambda_3 = \frac{1}{\lambda_1 \lambda_2}. \tag{2.4}$$

In order to describe the anisotropy of the axons, the stretch invariant I_4 was used:

$$I_4 = a_0 \cdot C \cdot a_0, \tag{2.5}$$

where a_0 is a vector describing the axonal orientation, which was defined by the measured θ_m for both the basic and structural models, and $C = F^T F$ is the right Cauchy-Green strain tensor.

The stress-stretch relationship for the basic model utilized a modified Ogden anisotropic hyperelastic strain energy density function (W) which has been shown to fit the stress-stretch relationship of brain white matter in uniaxial tension [Velardi et al. 2006]:

$$W = \frac{2\mu}{\alpha^2}(\lambda_1^\alpha + \lambda_2^\alpha + \lambda_3^\alpha - 3) + \frac{2k\mu}{\alpha^2}(I_4^{\alpha/2} + 2I_4^{-\alpha/4} - 3), \tag{2.6}$$

where the three parameters μ, α, and k represent the infinitesimal shear modulus, nonlinearity, and anisotropy, respectively. This function has been shown to fit the stress-stretch relationship of brain white matter in uniaxial tension [Velardi et al. 2006]. To determine the relationship between the axonal structure and the mechanical behavior of the biaxial specimens, the measured structural parameters κ and f_a were correlated to each of the fitted basic model parameters μ, α, and k using a linear regression.

The formulation of the structural model was derived from the linear regression between k and f_a. The k parameter from the basic model was replaced with ($k' f_a + k_0$), where k' is the new anisotropic model parameter, and k_0 is the intercept of the linear regression. The axonal distribution parameter (κ) acts to disperse the anisotropic alignment by replacing I_4 in the strain energy density function with the following term [Gasser et al. 2006]:

$$I_4 \Rightarrow (\kappa I_1 + (1 - 3\kappa)I_4) \tag{2.7}$$

where I_1 = trace(C) is the first strain invariant. When κ = 0, equation (2.7) reduces back to I_4, representing perfectly aligned axons. When κ = 1/3, equation (2.7) reduces to (1/3)I_1, representing perfectly isotropic behavior. With both f_a and κ incorporated, the structural model takes the final form:

$$W = \frac{2\mu}{\alpha^2}(\lambda_1^\alpha + \lambda_2^\alpha + \lambda_3^\alpha - 3) + (k' f_a + k_0)\frac{2\mu}{\alpha^2}[(\kappa I_1 + (1 - 3\kappa)I_4)^{\alpha/2} + 2(\kappa I_1 + (1 - 3\kappa)I_4)^{-\alpha/4} - 3]. \tag{2.8}$$

The structural parameters θ_m, κ, and f_a were defined for each specimen independently and incorporated into equation (2.8).

In order to fit the experimental data, the theoretical Cauchy stress (σ) of each model was calculated using the equation:

$$\sigma = 2J^{-1}F \cdot \frac{\partial W}{\partial C} \cdot F^T, \tag{2.9}$$

where J is the determinant of F and was set to unity in order to impose the condition of incompressibility. The experimental Cauchy stress in each direction was calculated as $\sigma_i = (P/A)\lambda_i$, where P is the force and A is the undeformed cross-sectional area. The models were fitted to the experimental data from each test using the *fmincon* function in MATLAB to minimize the percent error. The μ parameter was constrained to be greater than zero, while α and k were unconstrained. One set of model parameters (per model) was determined for each specimen by simultaneously fitting all five mechanical tests.

In order to test the robustness of the basic model and the value of using biaxial and uniaxial tests, predictions of the mean experimental data were made using model fits. The corpus callosum and corona radiata specimens were combined into a single data set, and experimental means were determined for each stress-stretch curve. The model was fitted to only the two uniaxial tests for each specimen individually, and the mean model parameters were used to predict the stress for the three biaxial tests (not used in the fits). Separately, the model was fitted to the three biaxial tests, and the mean model was used to predict the two uniaxial tests.

2.2.9 Probabilistic Analysis

A probabilistic analysis was performed to report the probability distribution of the fitted basic and structural models and to probe the effectiveness of the structural modeling approach to decrease the variability in the model (and thus improve the certainty of model predictions). The

statistical distribution of the fitted model parameters (μ, α, k, and k') was determined by fitting 17 candidate parametric distribution functions to the empirical probability distribution of the data using the *allfitdist* function available in MATLAB and choosing the best fit distribution. The *allfitdist* function ranks all candidate distributions according to multiple criteria, including the negative of the log likelihood, Bayesian information criterion, and Alkaike information criterion with a correction for finite sample sizes. The results were also checked visually for fits to the probability distribution and the cumulative distribution.

The chosen distribution and natural parameters (e.g. mean and standard deviation) of the model variables were used in the probabilistic analysis. NESSUS software (Southwest Research Institute, San Antonio, TX) was used to determine the effects of the fitted model parameter variability (*i.e.* scatter) on the resulting model stress predictions at given levels of stretch for equibiaxial and uniaxial stretches. A Monte Carlo sampling method of 100,000 samples was used to determine the cumulative probability function of the stress predictions at each given stretch. Additionally, the global sensitivity of the input variables on the predicted stress was determined using a variance decomposition method. The variance of the output is affected by the variance of the input parameters. The sensitivities include first order (direct) effects of each input parameter on the output variability, and higher order effects of the interaction between input parameters on the output variability. Each sensitivity effect can range between zero and one, and the sum of all sensitivities is equal to one.

2.2.10 Stress Correlation

Because of boundary effects and stress concentrations, the stress at the center of a specimen in a biaxial test is not equal to the mean stress through the grips. In other words, the stress in the region of interest is not equal to the force divided by the cross sectional area. The

stress in the region of interest can be estimated by finding a correlation factor via finite element modeling [Jacobs et al. 2013]. For an isotropic material in a cruciform geometry, this correlation factor is 0.76; however, this factor is dependent on material behavior/parameters such as anisotropy and Poisson ratio [Jacobs et al. 2013]. In order to calculate the stress in the biaxial tests, an initial correlation factor of 0.76 was applied to the Cauchy stress calculation. For each test of each specimen, the basic model was fitted to the new stress-stretch data, and the fitted model was implemented into a specimen-specific finite element model. This model was used to find the next iteration of the correlation factor in each direction for the mean stress in the region of interest. The constitutive model was re-fitted, and this process was iterated until convergence was achieved.

This should be regarded as an estimate derived from a finite element model prediction; it is not an empirical measurement of the local stress. This correlation factor is dependent on many variables, including the anisotropy and stretch in each direction, and any heterogeneity in the specimen makes the accuracy of this method intractable to discern. Because this correlation factor is not an established method, the basic model was also fitted to the data with no correlation factor and the data were reported herein in order to provide availability to both data sets.

2.3 Results

2.3.1 Strain Measurements

Strain maps demonstrated a high degree of homogeneity of the strain field in the central region of the specimens (Figure 2.5). Within the defined region of interest of each specimen, the mean and standard deviation of strains were measured. The average of the standard deviations within the region of interest was 18% of the mean strain (Table 2.1).

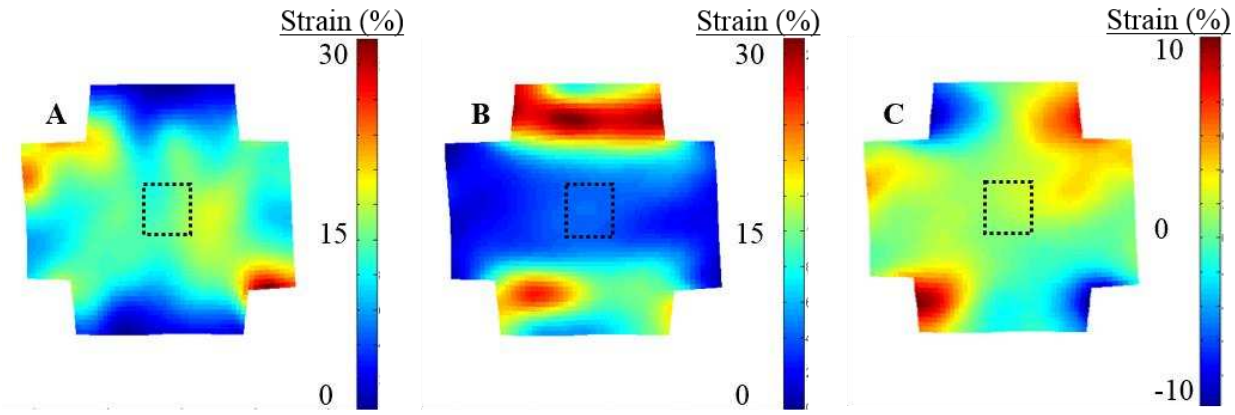

Figure 2.5: Typical strain maps from a 1:1 test showing strain (A) in the horizontal (axonal) direction, (B) the vertical (transverse) direction, and (C) the shear strain. The squares in the center represent the region of interest from which the mean stretches were measured.

Table 2.1: The mean strains measured within the region of interest. Standard deviations represent the average of standard deviations within the region of interest for each test (a measure of the homogeneity of the strain fields).

Loading ratio	Axonal strain (Mean ± S.D.)	Transverse strain (Mean ± S.D.)	Shear strain
1:1	0.151 ± 0.025	0.123 ± 0.024	0.023
1:05	0.160 ± 0.033	0.058 ± 0.017	0.019
05:1	0.083 ± 0.018	0.142 ± 0.028	0.019
Uniaxial Axonal	0.172 ± 0.026	-0.055 ± 0.012	0.013
Uniaxial Transverse	-0.053 ± 0.014	0.157 ± 0.026	0.009

The testing setup also effectively resulted in minimal shear, with a peak shear strain that was on average 11% of the greater of the two longitudinal strains. To determine the sensitivity of the longitudinal stress to the shear strain, the theoretical stress was calculated in each direction based on the mean fitted coefficients. For the calculations, the strains were set at the mean strains shown in Table 2.1 for each testing ratio. The shear strains were swept from 0 to 0.07 (the maximum shear strain measured in any single test). The percent difference from the zero-shear state was determined for each longitudinal stress. The uniaxial stretch in the axonal

direction was the loading case most sensitive to the shear strain. The measured shear strains had a mean impact of less than 1% on the resultant model stress; therefore, the assumption of negligible shear was deemed appropriate.

2.3.2 Biaxial Experiments and Modelling

The experimental results demonstrated a typical nonlinear hyperelastic shape to the stress-stretch curves. With the basic model fitted simultaneously to all five tests of each specimen, the mean percent error was 18%. The resulting parameters are reported both with and without the correlation factor applied to the data (Table 2.2), and the data with the correlation factor were used for the remainder of the analysis. The correlation factor was generally greater in the axonal direction than the transverse direction. In the axonal direction, the means in the 1:1, 1:0.5, 0.5:1, and uniaxial tests were 0.80, 0.86, 0.73, and 0.98, respectively. In the transverse direction the means were 0.77, 0.74, 0.80, and 0.85, respectively. Because of the greater stiffness in the axonal direction, there was a greater transfer of stress and strain to the central region of interest, which was also reflected in greater experimental strain measurements in the axonal direction (Figure 2.5, Table 2.1). None of the parameters were significantly different between the two regions ($p = 0.89$ for μ, $p = 0.97$ for α, and $p = 0.22$ for k, using a student's t-tests). With the two regions combined, the k parameter mean was significantly greater than zero ($p = 0.043$, using student's t-test), indicating that the average white matter tissue was stiffer in the axonal direction than in the transverse direction. However, the results for k were highly variable, and some specimens even had a negative value, indicating a stiffer response in the transverse direction.

When the basic model was fitted to the uniaxial data and used to predict the mean stress of the biaxial tests, and *vice versa*, these combined predictions had a mean percent error of 46%.

Table 2.2: Fitted model parameters for data with and without the correlation factor applied (mean ± standard deviation).

		μ (Pa)	α	k
Correlation factor	Corona radiata	480 ± 230	24 ± 6	0.14 ± 0.37
	Corpus callosum	460 ± 270	24 ± 6	0.54 ± .83
No correlation factor	Corona radiata	610 ± 290	23 ± 6	0.09 ± 0.49
	Corpus callosum	580 ± 350	23 ± 5	0.48 ± 0.74

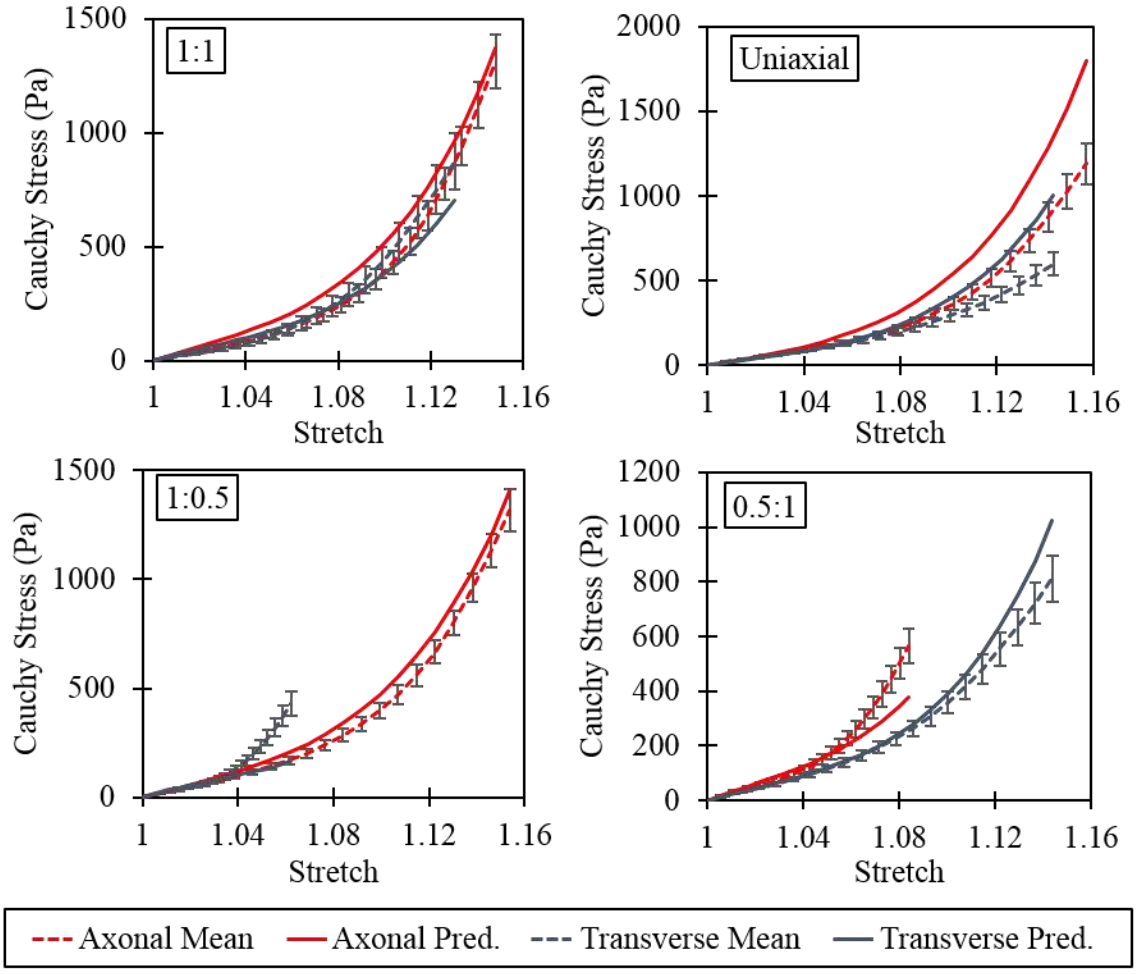

Figure 2.6: Model predictions of the mean experimental stress-stretch curves. The two separate uniaxial tests are shown together on a single plot. Error bars show standard error of the mean.

When the model was fitted to all 5 tests simultaneously, the predictions of the experimental data demonstrated a reduced error (26%), however, in many cases, these predictions also fell outside of one standard error envelope of the mean (Figure 2.6). Most notably, the model over-predicts the stress in both uniaxial tests and under-predicts the stress in the transverse direction of the 1:0.5 test.

2.3.3 Structural Analyses

Histology measurements showed that the mean angle θ was significantly greater for the corona radiata specimens than for the corpus callosum specimens ($p = 0.004$, Wilcoxon rank sum test); the mean ± standard deviation was 7.9 ± 6.8 degrees for the corona radiata and 1.4 ± 0.9 degrees for the corpus callosum. This confirms that the axons were generally well oriented in the direction of loading, especially for the corpus callosum specimens. The measured distribution κ was also significantly greater for the corona radiata specimens than for the corpus callosum specimens ($p < 0.001$, Wilcoxon rank sum test). The mean ± standard deviation was 0.066 ± 0.034 for the corona radiata and 0.012 ± 0.008 for the corpus callosum. The corpus callosum measurements demonstrate that κ approximates zero, indicating that the axons in the corpus callosum were highly aligned. Conversely, axonal orientations in the corona radiata were more distributed, which corresponds with an observed fan-like pattern, in which the axons were oriented radially. From TEM images, the measured f_a was nearly identical for the two regions; the mean ± standard deviation was 0.31 ± 0.06 for the corona radiata, and 0.32 ± 0.05 for the corpus callosum.

Even though there were significant regional differences in the orientation and distribution of axons, these differences were not manifested in the mechanical testing results. The fitted model parameters showed no differences between regions. However, the mechanical and

structural data were further analyzed on an individual specimen basis. Each measured structural property was plotted against each model parameter, and a linear regression was performed to determine if a correlation existed. While θ_m and κ showed no distinguishable correlations with any of the model parameters, f_a did have a significant positive correlation with the k parameter ($p < 0.001$, Fisher's Z transformation on the correlation coefficient) (Figure 2.7). The linear regression gave the relationship: $k = 9.0\, f_a - 2.6$, with a coefficient of determination of $r^2 = 0.58$.

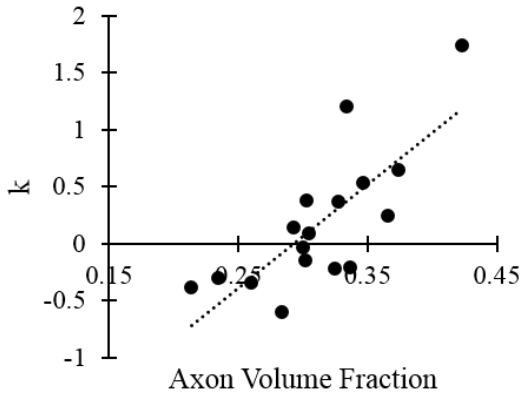

Figure 2.7: The measured axon volume fraction had a positive correlation with the anisotropic k model parameter. One data point was removed as a result of an outlier analysis.

2.3.4 Probabilistic Modeling

The formulation of the structural model was derived from the correlation between k and f_a, and k from the basic model was replaced with $(k' f_a - 2.6)$, matching the equation of the linear regression. The parameters for the basic model and structural model were used to find the best-fit statistical distributions, which were subsequently used to define the probabilistic analysis. For the basic model, μ exhibited a lognormal distribution with the mean of $\ln(\mu) = 6.1$ and the standard deviation of $\ln(\mu) = 0.53$ (with μ in Pa). The α parameter exhibited a Weibull distribution with the scale = 23 and the shape = 4.5. The k parameter exhibited a generalized

extreme value distribution with the shape = 0.18, scale = 0.44, and location = -0.071. For the structural model, μ exhibited a lognormal distribution with the mean of ln(μ) = 6.1 and the standard deviation of ln(μ) = 0.54 (with μ in Pa). The α parameter exhibited a Weibull distribution with the scale = 23 and the shape = 4.4. The *k'* parameter exhibited a normal distribution with the mean = 9.0 and standard deviation = 1.4.

The probabilistic analysis had a high variability in the stress predictions (Figure 2.8). A measure of variability was found by taking the differences between the 5% cumulative probability curve and the median (50% cumulative probability) curve, and between the 95% curve and the median curve. In an equibiaxial prediction, the variability in the axonal stress decreased by a mean of 13% from the basic model to the structural model, and the variability in the transverse stress increased by 6.8%. For the uniaxial predictions, it decreased by 16% in the axonal direction, and increased by 5.8% in the transverse direction.

Using the variance decomposition method, it was found that the basic model was much more sensitive than the structural model to the *k* (or *k'*) parameter (Figure 2.9). The sensitivities were dependent on the level of stretch. For both models at low stretch levels, the sensitivity to μ was very high, and the sensitivity to α was close to zero. At higher stretches, the sensitivity to μ decreased, and the sensitivity to α increased. This trend was expected because μ is representative of the infinitesimal modulus, and α is representative of the nonlinearity, therefore its effect on the model increases as stretch increases.

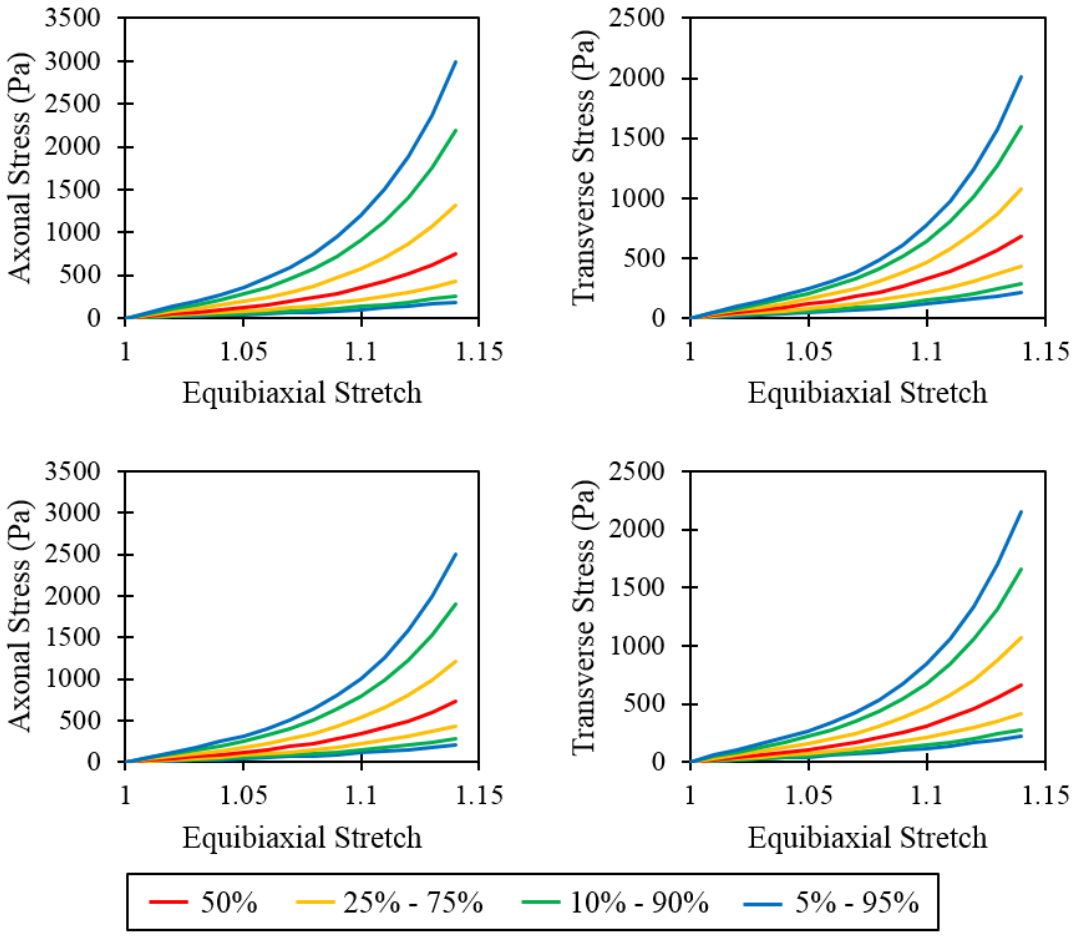

Figure 2.8: Stress predictions for an equibiaxial test at selected cumulative probability levels for the basic model (top) and the structural model (bottom). Uniaxial predictions showed very similar results.

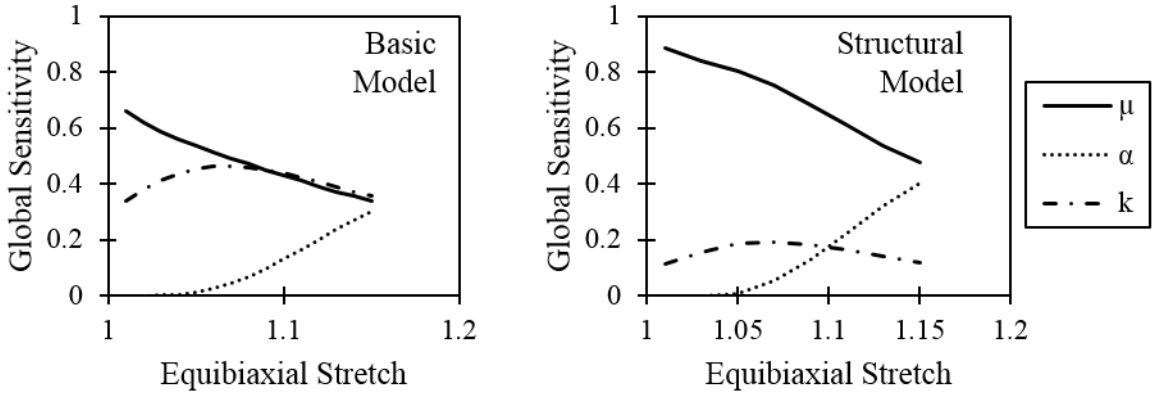

Figure 2.9: Global sensitivities of the model parameters on the basic and structural model stress predictions for an equibiaxial tests. These total sensitivities include direct effects and higher order interaction effects.

2.4 Discussion

2.4.1 Experiments and modeling

The current study was the first to investigate the biaxial tensile mechanics of brain white matter. The experimental design allowed for reliable specimen preparation from fresh tissue, and the testing setup successfully minimized shear strains and produced relatively homogeneous strain in the region of interest. The minimal shear strains that were present were likely due to imperfect symmetry in the testing setup, nonzero axon orientations (θ_m), or inhomogeneity in the tissue itself. The chosen anisotropic Ogden model was able to fit the data reasonably well, with a mean error of 18%. While this error may seem somewhat high for a model fit, it should be noted that the model was fitted to ten curves simultaneously (two directions of stress for each of five tests), and much of the error could be attributed to experimental variability between tests. More complicated model formulations were used in an attempt to better fit the data but showed little improvement in the fits and poorer predictions of the mean experimental data. A two-term Yeoh model with an exponential anisotropic term took the form:

$$W = C_{10}(I_1 - 3) + C_{20}(I_1 - 3)^2 + \frac{k_1}{k_2}(e^{(k_2(I_4-1)^2)} - 1), \tag{2.10}$$

where C_{10} is half the infinitesimal shear modulus, C_{20} is a nonlinear isotropic parameter, and k_1 and k_2 are the linear and nonlinear anisotropic parameters, respectively. The fits were only slightly better with this four-parameter model, at 16% error. The error of the predictions was higher, at 39%, compared to 26% for the three-parameter Ogden model. The Ogden model was therefore chosen as the simpler model that described the data well.

The first method of model predictions involved fitting the model to only some of the five tests done on each specimen. The model fitted to the three biaxial tests was used to predict the two uniaxial tests, and the model fitted to the uniaxial tests was used to predict the biaxial tests.

In the second method, all five tests were fitted, and the mean parameters were used to predict the mean experimental data of all tests. Since the data being predicted were used in the model fits in the latter case, the error was expected to be lower. However, the high 46% error of the first method of predictions suggests that uniaxial or biaxial tests alone are not sufficient for modeling the tensile behavior of white matter. The lower 26% error of the second method still demonstrates that using both uniaxial and biaxial data in the model fits improves the robustness of the model, or, its ability to predict multiple loading conditions.

The mean infinitesimal shear modulus, μ, calculated in the current study (470 Pa) was similar to previously reported values of 137 Pa for porcine corona radiata in uniaxial tension [Velardi et al. 2006], and 500 Pa for lamb corpus callosum in shear and indentation [Feng et al. 2013]. However, values for the same measure of k were greater in these studies than the current study, ranging from 1.77 to 13. Other studies in shear reported the corona radiata to be isotropic [Shuck and Advani 1972], have very low anisotropy [Nicolle et al. 2004], or even be stiffer in the transverse direction, while corpus callosum was stiffer in the axonal direction [Prange and Margulies 2002]. Differences in anisotropy may be attributed to the strain rate, the mode of loading (e.g. tension or shear) or the region of the brain. In the current study, k was greater for the corpus callosum region than for the corona radiata region (0.54 and 0.14, respectively), although the difference was not statistically significant. Although the value of k was found to be negative for some individual specimens, the smallest k value was -0.36. The model is positive definite for all $k > -1$, therefore, the range of model parameters found is valid. The negative values of k should be interpreted phenomenologically as representing a lower stiffness in the axonal direction. k does not directly represent the mechanical contribution of the axons, as they

would not contribute a negative stiffness. It is possible the transverse cellular interactions were stiffer than the axons in these samples.

Previous mechanical studies on brain tissue have had a high variability in their results, and surprisingly even in the shape of the stress-stretch curves. Different tensile tests have reported stress-stretch curves that were concave-up, concave-down, or nearly linear [Franceshini et al. 2006, Miller and Chinzei 2002, Rashid et al. 2014, Velardi et al. 2006]. The current results showed a concave-up shape to the curves and a corresponding mean α of 24, whereas uniaxial tests of white matter found α = 2.38-6.84 and curves that were nearly linear [Velardi et al. 2006]. These differences may depend on loading history of the tissue as well as strain rate [Franceshini et al. 2006, Miller and Chinzei 2002].

2.4.2 Structural analysis

The histology results showed that both θ_m and κ were both relatively low for the corpus callosum. The low mean orientation indicates that the axons were well oriented in the testing direction, which minimized shear strains while loading. The low distribution of axonal orientation indicates that the specimens were more homogeneous. Although θ_m and κ were both greater in the corona radiata, θ_m = 7.9 degrees is still relatively well aligned, and κ = 0.066 is much closer to perfectly aligned (κ = 0) than to perfectly isotropic (κ = 0.333). Despite the differences between the two regions, neither structural property correlated with any differences in mechanical testing results on either a regional or individual specimen basis.

The TEM analysis and f_a measurement had a few limitations. Measurements had to be taken from outside of the central region of interest of the specimen because that central region was being processed for histology. Also, the entire cross section of the specimen was not measured. Rather, a randomized sample of 18 images was used to estimate f_a. This estimation

likely added a factor of variability to the data. The TEM images showed axons with microstructures that had a considerable amount of damage. Control specimens, which originated from locations adjacent to the biaxially tested specimens and were fixed and processed at the same time as the tested specimens, demonstrated the same damaged microstructures and were visually indistinguishable from the tested specimens. It is likely that the observed damage was a result of autolytic post-mortem changes not incurred during the mechanical testing [Sheleg et al. 2008]. It is possible for the chemical processing to cause tissue shrinking during dehydration or embedding in resin [Bastacky et al. 1985, Kim et al. 1996], therefore, the absolute magnitude of the measured f_a should be viewed within this context. However, since all specimens followed the same fixation and processing procedure, the relative differences between specimens were not affected.

The difference in f_a between specimens did correlate with the anisotropic model parameter *k*. This indicates that the mechanical anisotropy of white matter is functionally related to the axonal volume fraction. Additionally, including f_a in the structural model did have some effect on the mean model parameters. While not *significantly* different ($p = 0.22$), the basic model's *k* parameter was 0.54 for the corpus callosum, and 0.14 for the corona radiata. The structural model's mean *k'* parameter was much more similar for the two regions (9.0 and 9.1 for the corpus callosum and corona radiata, respectively).

2.4.3 Probabilistic analysis

As seen through the probabilistic analysis, implementing the f_a measurement into the structural model did decrease the variability of the model predictions in the axonal direction. This is beneficial in improving the confidence of model predictions. The implementation of the structural material model into a computational model would require knowledge of the axon

volume fraction at different locations within the brain. Although obtaining this information is feasible through TEM or similar imaging studies, the average 14% decrease in variability in the axonal stress prediction is a somewhat small difference. Also, the variability in the transverse stress predictions increased slightly due to the inclusion of κ, which causes the anisotropic (axonal) term to contribute to the transverse stress. Therefore the variability in the anisotropic term had a slight effect on the transverse stress as compared to the basic model, in which only the isotropic term contributes to the transverse stress.

The statistical distribution of the model parameters and the cumulative probability distribution of the model stress predictions can be beneficial to computational modeling studies of the brain. It is often preferred for a computational model to predict the probability of an outcome rather than the mean outcome. An example is in the assessment of sports or automobile equipment in which it is necessary to predict the probability of suffering a traumatic brain injury as a result of an impact [Takhounts et al. 2008]. Previous work has demonstrated the probability of an axonal injury in a nerve relative to the level of strain [Bain and Meaney 2000]. However, this information alone would be incomplete in a computational study, and all other factors of variability should be used, including the variability of the constitutive material models.

2.4.4 Preconditioning

Mechanical tests on brain tissue are sometimes performed without preconditioning, due to the relatively compliant and delicate nature of the tissue [Miller and Chinzei 2002, Rashid et al. 2014, Velardi et al. 2006]. It could also be argued that preconditioning should not be performed because brain tissue is not loaded to high strains *in vivo* prior to a traumatic injury or surgical procedure. However, the brain is normally subjected to mechanical stresses *in vivo* due to fluctuating intracranial pressure [Steiner and Andrews 2006], as well as mechanical loads

induced by non-injurious accelerations of the head. For the biaxial tests, it was best to precondition the specimens prior to testing in order to obtain a repeatable response [Cheng et al. 2008], especially since the experiments included multiple tests of each specimen at different displacement ratios.

Some studies on brain tissue mechanics have reported both preconditioned (last cycle) and non-preconditioned (first cycle) properties [Gefen et al. 2003, Gefen and Margulies 2004, Prevost et al. 2011]. In order to determine the effects of preconditioning in the current study, the 1:1 test results from the experiment were compared to the results of the preconditioning regimen, which was also a 1:1 test at the same global displacement levels. The results of the fitted basic Ogden model were compared for a total of four groups: the first cycle of preconditioning (P1), the last (fifth) cycle of preconditioning (P5), and the first and last cycles of the 1:1 test (T1 and T5, respectively). The resulting parameters can be found in Table 2.3. The P1 cycle was the only loading cycle with no previous loading history (no preconditioning), and this cycle had a significantly larger μ parameter than all other loading cycles ($p < 0.01$, using a one-way ANOVA on log-transformed data with a Bonferroni-corrected paired t-test). This result demonstrated that the preconditioning regimen decreased the measured stiffness of the tissue, a commonly observed phenomena in biological soft tissues. The α parameter was lower for P1 than the other three cycles, indicating a more linear relationship between stress and stretch ($p < 0.01$, using a one-way ANOVA with a Bonferroni-corrected paired t-test). The k parameter showed no significant differences between groups (using a paired Wilcoxon rank sum test).

Because one purpose of preconditioning is to improve data consistency, the final cycle of the preconditioning regimen (P5) should ideally produce the same results as the final cycle of the 1:1 test (T5). The greatest difference between these two loading cycles was observed in the μ

parameter, which was 14% lower for the T5 test than for the P5. However, none of the parameters were significantly different ($p = 0.9$ for μ, $p = 0.2$ for α, and $p = 0.73$ for k), and considering the inherently high variability in the data, it is our position that the preconditioning regimen was sufficient for producing consistent, reliable results.

Table 2.3: Fitted model parameters comparing the first (P1) and fifth (P5) cycles of the preconditioning regimen and the first (T1) and fifth (T5) cycles of the 1:1 test (mean ± standard deviation). The correlation factor was not applied to these data.

	μ (Pa)	α	k
P1	1700 ± 840	19 ± 6	-0.15 ± 0.50
P5	750 ± 380	27 ± 7	0.40 ± 1.34
T1	760 ± 400	26 ± 6	0.14 ± 0.97
T5	650 ± 220	31 ± 8	0.40 ± 1.72

2.4.5 Using ovine tissue as a model for the human brain

Due to the fast degradation of brain tissue post-mortem, it is very challenging to test fresh human tissue. Therefore, the large majority of mechanical experiments use animal brain specimens. There are no mechanical studies systematically comparing ovine tissue to human tissue. It has been reported that modeling of human tissue tested in tension, compression, and shear produced an infinitesimal shear modulus of 900-1650 Pa [Moran et al. 2014], which may be greater than the current study because the tissue was tested on average four days post mortem [Jin et al. 2013]. One study obtained a limited sample of fresh human grey matter from lobectomy procedures and tested it in shear [Prange and Margulies 2002]. The mean infinitesimal shear modulus (300 Pa) was very similar to the previously reported experimental mean of ovine grey matter in shear (290 Pa) [Feng et al. 2013]. Even though human and ovine tissue testing data are limited and taken from separate studies, this degree of correspondence

provides *de facto* evidence that ovine tissue is reasonably representative of human tissue. Although smaller in size, the gross anatomy of the ovine brain is very similar to humans, with both having large proportions of cerebral white matter [Duncan et al. 2002, Silbereis et al. 2010]. This is not true in rodents and other small animals. The basic cellular structure is similar between sheep and humans, although humans have larger neurons on average, which is typical for larger brain sizes [Herculano-Houzel 2014]. Additionally, sheep are commonly used as a model for developmental brain disorders because the structure and the sequence of their brain development is similar to that of humans [Back et al. 2012, Silbereis et al. 2010].

2.5 Conclusions

This study expands upon the many previous mechanical studies of brain tissue to include biaxial tension, and the results demonstrated that including biaxial loading in addition to uniaxial loading improved the accuracy of model predictions. The corona radiata and corpus callosum demonstrated no conclusive differences in their mechanical behavior, despite differences in axon orientation and distribution. The tested white matter exhibited a mean anisotropic behavior, but the degree of anisotropy was relatively low compared to previous studies. The axon volume fraction demonstrated a positive correlation with the mechanical anisotropy. However, implementation of the axon volume fraction into the structural model only resulted in a small decrease in the uncertainty of model predictions.

3. VISCOELASTICITY OF BRAIN WHITE MATTER IN BIAXIAL TENSION[2]

3.1 Introduction

Computational models of the brain are important for their use in the development and simulation of neurosurgeries, operation planning, and registration of intraoperative brain shifts [Ferrant et al. 2001, Garcia et al. 2012, Miller et al. 2010, Miller 2011]. These models rely on accurate characterization of the brain tissue mechanical behavior. Due to the relatively low loading rates in surgical simulations, many models utilize constitutive equations derived from quasi-static experiments. However, viscoelastic effects are important, even at low strain rates, and viscoelastic characterization has been recommended to improve model predictions [Kyriacou et al. 2002].

Computational models of the brain often use linear viscoelastic material models [Post 2012, Zhang 2001]. However, these models are only valid at infinitesimal strains (less than 1%) due to the nonlinear relationship between stress and strain at finite deformations [Nicolle et al. 2004], and finite deformations commonly occur during surgical procedures such as catheter injections for convection enhanced delivery [Garcia et al. 2012]. Quasi-linear viscoelastic (QLV) formulations have been frequently used to model brain and other soft tissues due to their simplicity and ability to model nonlinear elastic behavior [Elkin et al. 2011, Laksari et al. 2012, Rashid et al. 2014]. However, QLV does not account for nonlinearities in the time-dependent response with respect to strain, and many biological tissues exhibit such nonlinearities, and accordingly, require fully nonlinear viscoelastic models [Shetye et al. 2014, Troyer and Puttlitz

[2] *This chapter has been submitted for publication in the Journal of the Mechanics and Physics of Solids.*

2011]. For modeling brain tissue, there is some evidence to suggest that QLV is sufficient in shear [Nicolle et al. 2004] and indentation [Elkin et al. 2011], however fully nonlinear models may result in improved fits to experimental data [Hrapko et al. 2006].

Due to the alignment of axons, white matter exhibits anisotropy in its relationship between stress and strain [Feng et al. 2013, Labus and Puttlitz 2016, Velardi et al. 2006]. It is possible for the time-dependent behavior to also be anisotropic. For example, the rate of relaxation may be different in the axonal direction relative to orthogonal directions. Tensor formulations of the reduced relaxation function in a QLV model have been used to investigate anisotropy in biaxial stress relaxation tests of heart valves [Grashow et al. 2006] and urinary bladders [Nagatomi et al. 2004]. However, the viscoelasticity of brain tissue has not been studied in biaxial loading states. Viscoelastic studies of brain tissue have investigated the anisotropy of the shear modulus in linear viscoelastic formulations [Abrogast and Margulies 1999, Feng et al. 2013, Ning et al. 2006], however, this approach does not provide the anisotropy of the time-dependent behavior.

Computational models typically utilize material models derived from experimental mean data and lack information on the inherent variability of the material properties. Probabilistic modeling approaches consider the variability of these model inputs in order to provide a full distribution of model predictions. Computational modeling studies of the brain can use probabilistic analyses to quantify the probability of an outcome of interest in a surgical procedure may better predict the anticipated local mechanics amongst the general population.

The purpose of this study was to characterize the viscoelastic behavior of brain white matter using biaxial stress-relaxation experiments. Specifically, the experiments were designed to determine if QLV is sufficient for modeling the viscoelasticity and to test the anisotropy of

both the elastic and time-dependent components of brain tissue. A best fit model was determined from the mean experimental data, and a probabilistic analysis was used to quantify the variance in model parameters and predictions.

3.2 Methods

3.2.1 Experimental Setup

The tissue dissection and experimental setup followed a previously described methodology (sections 2.2.1-2.2.3) [Labus and Puttlitz 2016]. In brief, a total of 12 ovine brain tissue specimens were dissected immediately (less than one hour) after animals were euthanized for unrelated studies. The corpus callosum was isolated from each intact brain, and slices were cut using a scalpel to separate the corpus callosum from the adjacent grey matter. A cruciform shape was punched from the resulting slice such that the dominant axonal direction was coincident with one of the loading directions. The cross-sectional area was determined in order to conduct *post hoc* calculations of the stress. The mean thickness was 1.7 mm, and the mean width was 6.9 mm.

A foam grip was attached with a cyanoacrylate adhesive to each of the four arms of the cruciform-shaped specimens in order to float the specimens on the surface of a saline bath, ensuring hydration throughout the test. Wires were used to connect two of the grips to linear actuators (T-LLS, Zaber Technologies Inc., Vancouver, BC, Canada), and the remaining two grips were connected to 250 gram capacity load cells (Model 31, Honeywell Sensotec, Columbus, OH). To track deformations, specimen surfaces were textured with graphite powder, and images were recorded at 100 frames per second. A MATLAB-based digital image correlation algorithm was used calculate the mean deformation gradient tensor in a 15x15 mesh grid covering a 2.4 mm square in the center of the specimen. The experimental Cauchy stress in

each direction was calculated as $\sigma_{ii} = c(P/A)\lambda_i$, where P is the force, A is the undeformed cross-sectional area, and λ_i is the stretch (diagonal elements of the deformation gradient tensor). A stress correlation factor was used to estimate the stress in the center of the specimen due to the boundary effects on stress in a biaxial test [Jacobs et al. 2013]. The correlation factor was determined via finite element analysis, following the procedure outlined in section 2.2.10 [Labus and Puttlitz 2016].

3.2.2 Experiments

Considering the post-mortem changes in brain tissue mechanics [Garo et al. 2007], experiments were limited to five stress relaxation tests and two cyclic tests, and the relaxation time was set to 100 s so that the testing for each sample was completed in two hours, and all tests were completed within six hours post-mortem. Specimens were initially loaded to a preload of 1.0 mN (mean stress of 85 Pa), followed by an initial preconditioning regimen of 20 cycles at equibiaxial displacements of 3.0 mm. In order to investigate the strain magnitude effects on the viscoelastic response, the experiment consisted of five biaxial stress-relaxation tests at equibiaxial displacements of 1.0, 1.5, 2.0, 2.5, and 3.0 mm. These displacements corresponded to mean strains of 3.6%, 6.0%, 9.1%, 12.0%, and 15.0%, respectively, in the axon direction, and 5.4%, 8.3%, 11.8%, 14.9%, and 18.3%, respectively, in the transverse direction. A loading rate of 6 mm/s (mean strain rate of 33% s^{-1}) was used for the ramp, and the final displacement was held for a relaxation time of 100 s. Additionally, two cyclic tests of 20 cycles each were conducted at equibiaxial displacements of 1.5 and 2.5 mm. The cyclic tests used the same loading rate of 6 mm/s. The order of the seven tests was randomized, and a recovery time of 1000s was used between each test [Duenwald et al. 2009, Shetye et al. 2014].

3.2.3 Quasi-linear viscoelastic modeling

To check the QLV assumption of a linear time-dependent behavior, the stress during the relaxation period of the experiments was plotted with logarithmic time and stress scales. The resulting slope of the curves is the relaxation rate, η. A relaxation rate that is dependent on the magnitude of stretch would imply that fully nonlinear viscoelasticity is required to model the behavior. However, for a constant relaxation rate, QLV would be valid. Because η was shown not to depend on stretch (Figure 3.1), a QLV formulation was used for subsequent modeling.

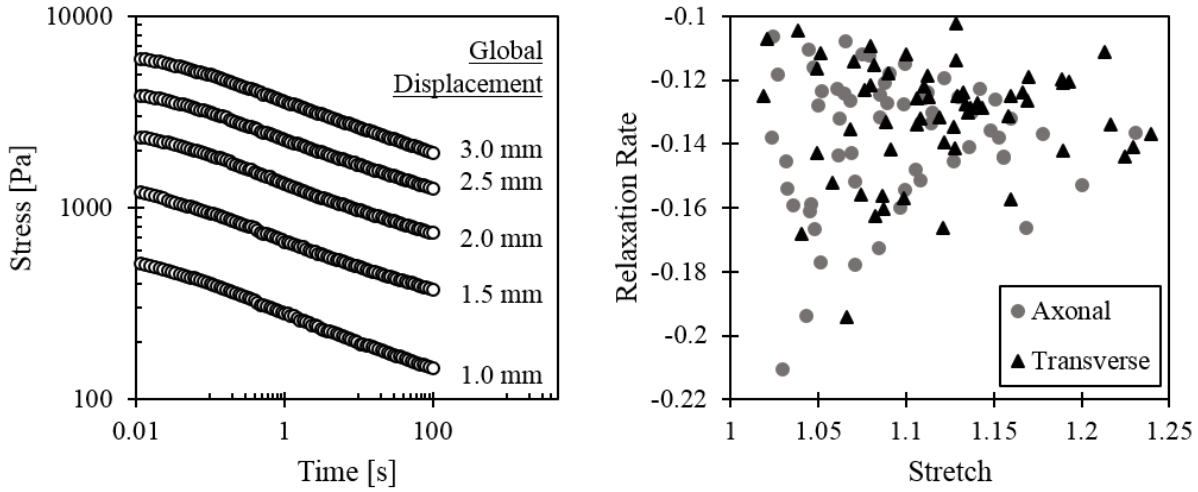

Figure 3.1: Left: The relaxation curves plotted on a log-log scale show a constant relaxation rate (slope) that does not depend on strain magnitude. Right: The normalized relaxation rates for all curves show no correlation relative to the measured stretch.

The QLV formulation for Cauchy stress (σ_{ij}) in three dimensions can be written as:

$$\sigma_{ij}(\varepsilon, t) = \int_0^t G_{ijkl}(t-\tau)\frac{\partial \sigma_{ij}^e[\varepsilon_{kl}(\tau)]}{\partial \tau} d\tau + \sigma_0 \tag{3.1}$$

where $\varepsilon_{kl}(\tau)$ is the applied strain, t is time, $G_{ijkl}(t)$ is the reduced relaxation tensor, σ_{ij}^e is the instantaneous elastic stress, τ is a time variable of integration, and σ_0 is the initial stress. To simplify the numerical integration, equation (3.1) can be integrated by parts:

$$\sigma_{ij}(\varepsilon,t) = \frac{\partial \sigma_{ij}^{e}(\varepsilon)}{\partial \varepsilon_{kl}}\left[-\int_0^t \frac{dG_{ijkl}(t-\tau)}{d\tau}\varepsilon_{kl}(\tau)d\tau + G(t-\tau)\varepsilon_{kl}(t) - G(t-0)\varepsilon_{kl}(0)\right] + \sigma_0 \tag{3.2}$$

The instantaneous elastic stress was derived from an anisotropic Ogden strain energy density function (W):

$$W = \frac{2\mu}{\alpha^2}(\lambda_1^{\alpha} + \lambda_2^{\alpha} + \lambda_3^{\alpha}) + \frac{2k\mu}{\alpha^2}(I_4^{\alpha/2} + 2I_4^{-\alpha/4} - 3), \tag{3.3}$$

where the three parameters μ, α, and k represent the infinitesimal shear modulus, nonlinearity, and anisotropy, respectively. With negligible shear, as demonstrated in previous quasi-static experiments using the same experimental setup (section 2.3.1) [Labus and Puttlitz 2016], the principal stretches λ_i are the diagonal elements of the deformation gradient tensor, measured through digital image correlation. With the axons aligned in the 1 direction, the anisotropic invariant I_4 is equal to λ_1^2. Following the assumption of incompressibility, the out-of-plane stretch λ_3 was found by:

$$\lambda_3 = \frac{1}{\lambda_1\lambda_2}. \tag{3.4}$$

In the case of biaxial tension, the instantaneous Cauchy stress in the axonal direction (σ_{11}^e) and the transverse direction (σ_{22}^e) were:

$$\sigma_{11}^e = \frac{2\mu}{\alpha}[\lambda_1^{\alpha} - (\lambda_1\lambda_2)^{-\alpha} + k(\lambda_1^{\alpha} - \lambda_1^{-\alpha/2})] \tag{3.5}$$

$$\sigma_{22}^e = \frac{2\mu}{\alpha}[\lambda_1^{\alpha} - (\lambda_1\lambda_2)^{-\alpha}] \tag{3.6}$$

and ε_{ii} in equation (3.2) is equal to $\lambda_i - 1$.

In the two-dimensional case, with shear assumed to be negligible, $G_{ijkl}(t)$ reduces to four functions: $G_{1111}(t)$, $G_{1122}(t)$, $G_{2211}(t)$, and $G_{2222}(t)$. Furthermore, the use of a strain energy

function requires major symmetry, where $G_{1122}(t) = G_{2211}(t)$. Each reduced relaxation function was approximated by the Prony series:

$$G(t) = G_\infty + \sum_{i=1}^{4} G_i e^{-t/\tau_i} \tag{3.7}$$

such that:

$$G_\infty + G_1 + G_2 + G_3 + G_4 = 1 \tag{3.8}$$

Where G_∞ is the long term relaxation coefficient, and G_i are relaxation coefficients corresponding to the time constants τ_i.

The time constants were determined from the relaxation time distribution spectrum obtained through an inverse Laplace transform performed in MATLAB. The spectrum was mapped on the time scale ranging from 10^{-4} s (on tenth of the resolution of the data, collected at 1000 Hz) to 10^3 s (ten times the relaxation time). A parametric study showed the results to be insensitive to the boundary locations beyond this range. There were typically multiple peaks in the relaxation time spectrum corresponding to events that reflect the relaxation behavior. Every curve had a peak greater than the 100s relaxation time, which is accounted for by the G_∞ coefficient of the model. Time constants τ_i were defined at the local maximum of each peak that occurred at less than 100s. This was done individually for each direction of stress and for each stress-relaxation test. The majority (89%) of relaxation curves resulted in four peaks, while the remainder resulted in five. The time constants from the curves with four peaks were averaged on a logarithmic scale, and these averages were used for all modeling: $\tau_1 = 0.021$, $\tau_2 = 0.26$, $\tau_3 = 2.7$, and $\tau_4 = 21$. No significant differences were observed in the values of the time constants between the axonal and transverse directions, or between the different strain magnitudes (One-Way ANOVA on logarithmic scale).

3.2.4 Anisotropy of reduced relaxation tensor

The QLV model was initially fitted to the experimental data assuming an instantaneous strain application. This assumption allows the model to be simplified so that equation (3.7) was fitted to the relaxation period, normalized to the peak stress, to find $G(t)$, and equations (3.5) and (3.6) were fitted to the ramping period. Because equation (3.7) is independent of strain, the relaxation tensor was reduced to two functions: $G_A(t)$ and $G_T(t)$ to describe the relaxation of the stress in the axonal and transverse directions, respectively. For each specimen, all five tests were fitted simultaneously using the fmincon function in MATLAB to get a single set of G_A and G_T coefficients. Due to the disproportionally large number of datum points in the long-term relaxation, the fitting algorithm minimized a weighted root-mean-squared (RMS) error that used a weighting function:

$$w_{relax}(t_n) = \frac{e^{-t_n/\tau_1} + e^{-t_n/\tau_2} + e^{-t_n/\tau_3} + e^{-t_n/\tau_4}}{4} \tag{3.9}$$

where t_n is the time during the relaxation period such that the peak stress occurs at t_n = 0s. This weighting function was first multiplied by the model error, and the root-mean-square of the weighted error was calculated.

This fitting procedure resulted in very small differences between the G_A and G_T coefficients, therefore, the model was simplified to assume the time-dependent behavior is isotropic, and just one reduced relaxation function was required: $G_{iso}(t) = G_{1111}(t) = G_{1122}(t) = G_{2211}(t) = G_{2222}(t)$. The same fitting procedure assuming an instantaneous strain application was repeated with this isotropic relaxation model, and all subsequent modeling used $G_{iso}(t)$.

3.2.5 Full-integral model fitting

In stress relaxation tests, viscoelastic models that assume an instantaneous strain application or a purely linear strain application during the ramping period have been shown to be poor predictors when applied to an actual experimental strain history [Abramowitch and Woo 2004, Troyer et al. 2012a, Sheyte et al. 2014]. Therefore, equation (3.2) was used to model the entire experimental stress-relaxation tests, using the measured strain history, including the ramping period and the creep in strain that occurred during the relaxation period. The fitting algorithm minimized a weighted error such that the ramping period and the relaxation period were weighted equally [Abramowitch and Woo 2004]. Since the relaxation period had its own weighting function, $w_{relax}(t_n)$, the ramping period required a similar function to scale the errors. Unlike $w_{relax}(t_n)$, this function applied the same weight to all datum points and was defined as: $w_{ramp} = mean[w_{relax}(t_n)]$. The final weighted error function, $RMSE_w$, that was minimized was:

$$RMSE_w = 0.5 * RMS[w_{ramp}(\sigma_{ramp,m} - \sigma_{\mathrm{ramp,e}})] + 0.5 * RMS[w_{relax}(t_n) \cdot (\sigma_{rel,m} - \sigma_{\mathrm{rel,e}})] \quad (3.10)$$

where *RMS* is the root-mean-squared operation, $\sigma_{ramp,m}$ and $\sigma_{\mathrm{ramp,e}}$ are the model and experimental stresses in the ramping period, respectively, and $\sigma_{rel,m}$ and $\sigma_{\mathrm{rel,e}}$ are the model and experimental stresses in the relaxation period, respectively.

In order to fit the peak stress of the curves such that an accurate reduced relaxation function was obtained, it was necessary to fit equation (3.2) to each of the five tests individually. From this, the mean parameters G_1, G_2, G_3, G_4, and G_∞ were calculated. Even though these parameters were fairly consistent, subtle differences in the shape of the ramping period between tests resulted in highly variable parameters for the Ogden model, especially μ and α. Therefore,

the relaxation function parameters were fixed at their fitted means, and the model was fitted a second time to all five tests simultaneously to determine μ, α, and k. To get a single set of parameters to describe the mean behavior, this fitting procedure was conducted to fit the averaged experimental stress-relaxation curves. The resulting average model was used to create predictions of the averaged data from the two cyclic experiments.

3.2.6 Probabilistic analysis

The full-integral fitting procedure described above was also conducted for each individual specimen. The statistical distribution of each fitted model coefficient was determined using the *allfitdist* function in MATLAB to fit candidate parametric distribution functions to the empirical probability distribution for that coefficient. Parametric distribution functions were chosen according to rankings of the Alkaike information criterion with a correction for finite sample sizes, as well as a visual inspection of fits to the probability distribution.

The resulting distributions and natural parameters (e.g. mean and standard deviation) were used to define the inputs of a probabilistic analysis in NESSUS (Southwest Research Institute, San Antonio, TX). The probabilistic analysis determined the effects of the input variability on the model stress predictions for a stress-relaxation test at an equibiaxial stretch of 1.1. A Monte Carlo sampling method of 100,000 samples was used to estimate the predicted stress at pre-determined cumulative probability levels of 5%, 10%, 25%, 50%, 75%, 90%, and 95%, at given times ranging from the time at peak stress (beginning of relaxation period) to 100s of relaxation. The global sensitivity of the input parameters on the variability of the predicted stress was determined using a variance decomposition method.

3.3 Results

3.3.1 Strain-dependence of relaxation

As mentioned in the Methods section above, the QLV assumption of linear time-dependent behavior was checked by measuring the relaxation rate of each relaxation curve. As shown by the plotted stresses of an example specimen, the relaxation rate did not appear to depend on the magnitude of strain (Figure 3.1). With all tests combined, the relaxation rate showed no correlation with measured stretch, and there was no significant difference in the relaxation rate between the 5 displacements tested (One-Way ANOVA, $p = 0.64$). The only visible trend in the relaxation rate is the greater variability at lower stretch levels, which is likely due to the lower signal to noise ratio in the measured stress at these lower stretch levels.

3.3.2 Anisotropy of reduced relaxation tensor

When fitted to the relaxation period of the curves assuming a Heaviside strain application, the QLV model fit the data well at all five stretch levels (Figure 3.2). When two reduced relaxation functions were used, the mean percent error was 5.6%, and the mean RMSE was 72 Pa. G_∞ was significantly lower for the axonal direction than the transverse direction, and G_2 was significantly greater for the axonal direction (Figure 3.3). Taken together, these results indicate that the axonal stress experienced greater relaxation than the transverse stress, and this difference primarily occurred near the time point of 0.26s. However, the numerical differences between the mean parameters, although statistically significant for some, were small. The maximum percent difference of 9.5% occurred at G_2. When comparing the normalized relaxation rates (Figure 3.1), the mean and standard deviation in the axonal and transverse directions were 0.139 ± 0.021 and 0.132 ± 0.018, respectively ($p < 0.01$, paired t-test). Despite the statistical significance, the numerical difference between means was again very small. When

only one reduced relaxation function, G_{iso}, was used, the model appeared to fit the relaxation curves well in both directions of stress and at all five stretch levels (Figure 3.2). The errors in the model fits remained low (mean percent error = 6.5%, mean RMSE = 76 Pa).

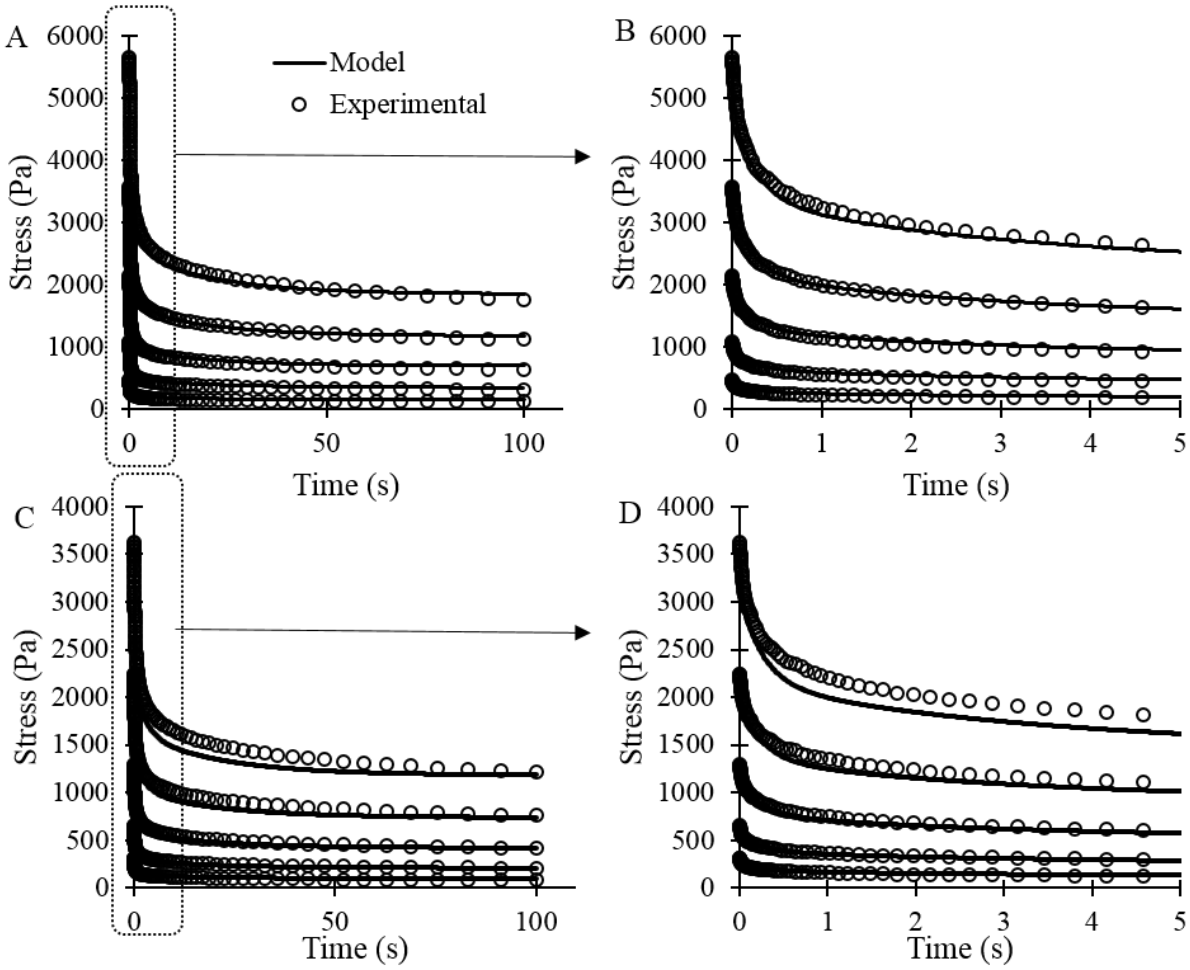

Figure 3.2: Fits of the G_{iso} QLV model to the experimental data, assuming an instantaneous strain application. Fits are shown for the axonal direction (A,B) and the transverse direction (C,D). Plots in (B) and (D) demonstrate the relaxation behavior in in the acute time frame (first 5s) after loading.

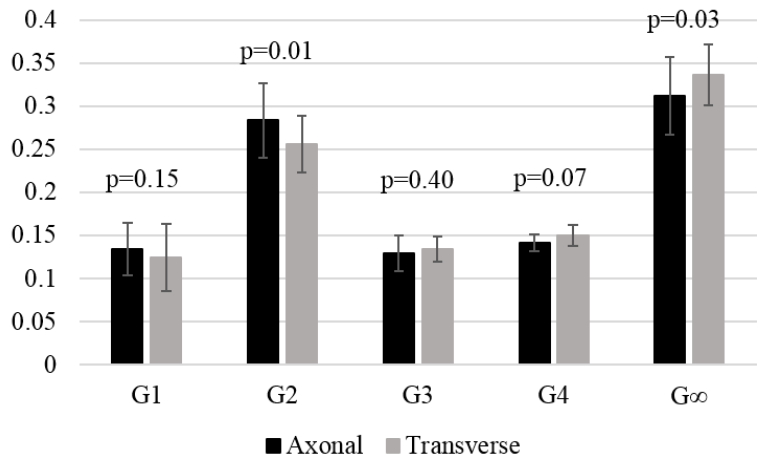

Figure 3.3: $G_A(t)$ compared to $G_T(t)$ found from model fits assuming an instantaneous strain application. p-values show results from paired t-tests.

3.3.3 QLV full-integral model fits and cyclic test predictions

The final fits of the full-integral QLV model (equation 3.2) to the entire stress-relaxation curves, using the full strain history, showed very good agreement for both the ramping period and the relaxation period (Figure 3.4). The QLV model was able to fit the experimental data at all five displacement magnitudes, and the simplification of using a single isotropic reduced relaxation function was satisfactory in fitting the relaxation in both directions of stress. The model fits had a mean RMSE of 220 Pa, which corresponded to 8.9% of the mean peak stress. When fitted to the averaged experimental data, the resulting coefficients represent a best-fit mean model (Table 3.1). The reduced relaxation function coefficients demonstrated a relatively high degree of relaxation that occurs at early time points, with G_1 being the greatest, followed by G_2, whereas G_3, G_4, and G_∞ were all relatively small. The Ogden model coefficients (μ, α, and k) represent the instantaneous elastic response, and the positive k coefficient indicates anisotropy with the axonal direction stiffer than the transverse direction.

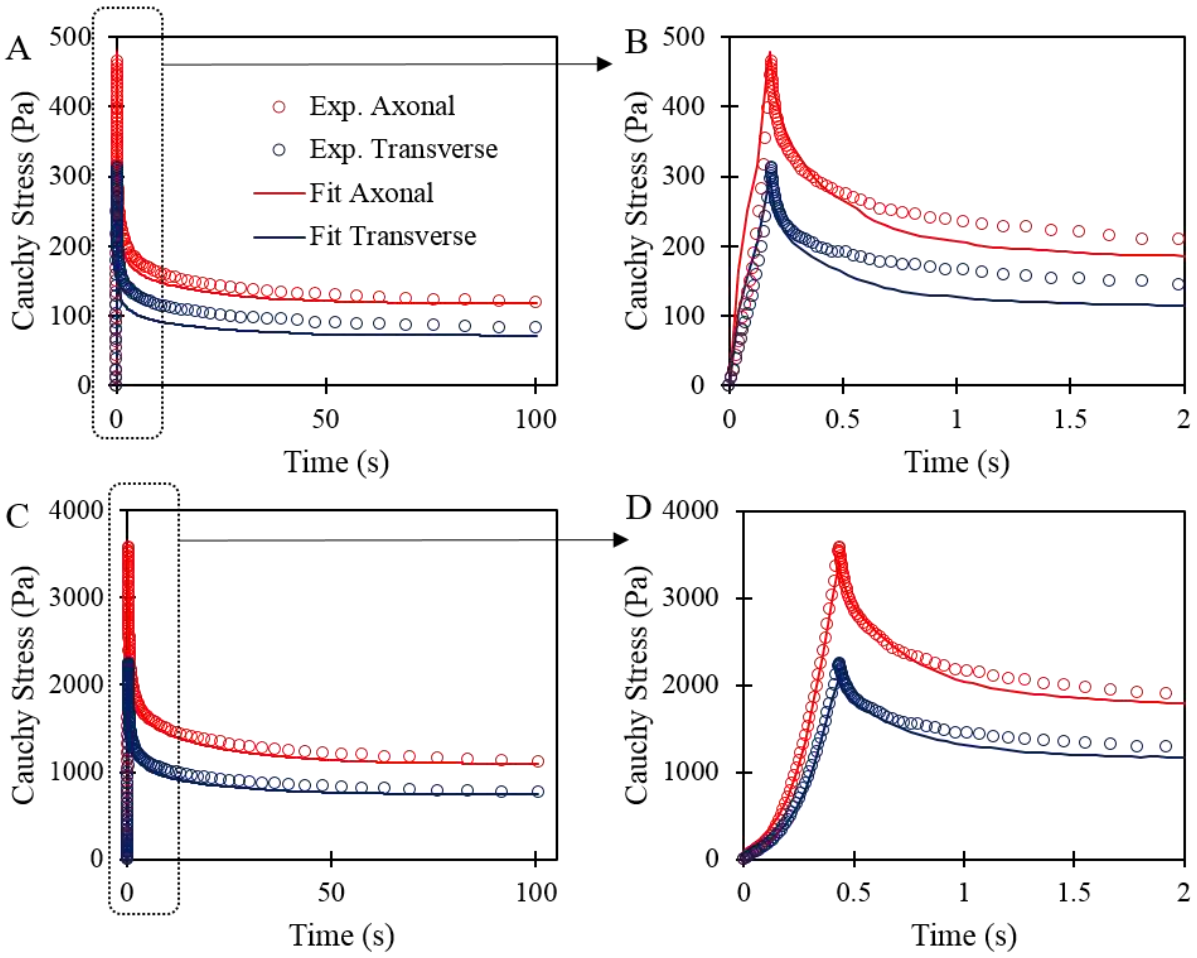

Figure 3.4: Fits of the full-integral QLV model with a single isotropic reduced relaxation function to experimental stress-relaxation tests. Examples shown for the (A) 1.0 mm test with an expanded view of the first 2s of the ramping and relaxation (B), and fits for the 2.5 mm tests (C and D).

These model fits included the full strain history of the experimental data, including during the relaxation period. Even though the global displacement was held constant during the relaxation period of the experiments, there was some measured creep, or increase in strain, in the central region of interest. In the axonal direction, the increase in strain from the beginning to the end of the relaxation period was 0.76% ± 0.54%, 0.91% ± 0.44%, 1.1% ± 0.65%, 1.3% ± 0.79%, and 1.4% ± 0.54% (mean ± standard deviation) for the 1.0mm, 1.5mm, 2.0mm, 2.5mm, and 3.0mm displacement tests, respectively. In the transverse direction, the increase in strain was

0.72% ± 0.72%, 1.0% ± 0.49%, 1.3% ± 0.68%, 1.7% ± 0.45%, and 2.2% ± 0.66% for the 1.0mm, 1.5mm, 2.0mm, 2.5mm, and 3.0mm displacement tests, respectively.

Table 3.1: Fitted model coefficients for the mean experimental data, and statistical distributions of the coefficients fitted to individual specimens.

	Full-integral model: mean experimental data	Statistical distribution	Natural parameters
G_1 (τ_1 = 0.021)	0.708	normal	Mean = 0.64 S.D. = 0.089
G_2 (τ_2 = 0.26)	0.179	normal	Mean = 0.21 S.D. = 0.055
G_3 (τ_3 = 2.7)	0.031	lognormal	Mean(ln(x)) = -3.2 S.D.(ln(x)) = 0.28
G_4 (τ_4 = 21)	0.032	lognormal	Mean(ln(x)) = -3.3 S.D.(ln(x)) = 0.33
G_∞	0.050	lognormal	Mean(ln(x)) = -2.7 S.D.(ln(x)) = 0.37
μ (Pa)	3400	lognormal	Mean(ln(x)) = 8.0 S.D.(ln(x)) = 0.47
α	17	normal	Mean = 17 S.D. = 2.6
k	1.9	lognormal	Mean(ln(x)) = 0.66 S.D.(ln(x)) = 0.69

The model fitted to the averaged experimental stress-relaxation tests was then used to predict the stress from the cyclic experiments. The model was able to accurately predict the mean experimental stress in both directions for both the 1.5mm and 2.5mm displacement tests (Figure 3.5). At the peak of each cycle, the predicted stress was within one standard error of the mean of the experimental data. However, after the first cycle, the model slightly over-predicted the stress in the early (initial ramping) phase of each cycle. These predictions had a mean RMSE of 130 Pa, which corresponds to 6.6% of the mean peak stress. The predicted stress was less than zero at the end of each cycle, however, the experimental apparatus was not designed to

measure compressive loads. Therefore, any predictive negative stresses were constrained to be equal to zero for the purpose of comparison to the experimental data.

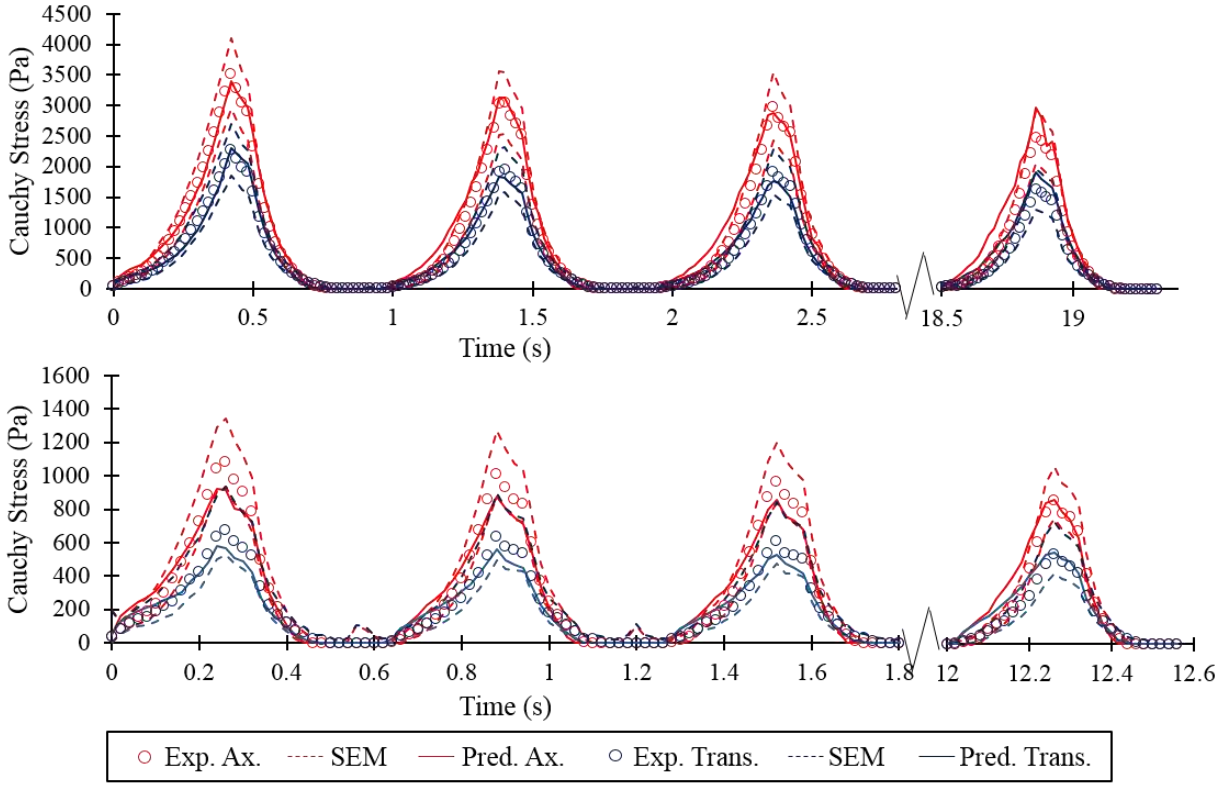

Figure 3.5: Model axonal and transverse stress predictions of the experimental cyclic tests, showing cycles 1, 2, 3, and 20 for the 2.5 mm displacement tests (top) and 1.5 mm displacement test (bottom). The experimental means and standard errors of the mean are shown.

3.3.4 Probabilistic analysis

In addition to fitting the full-integral QLV model to the averaged experimental stress-relaxation tests, each specimen was fitted individually. The best-fit statistical distribution function and natural parameters were determined for each parameter (Table 3.1). Many of the parameters demonstrated correlations with each other. Pearson's correlation coefficient (r) was determined for each pair of model parameters (Table 3.2) and included as an input in the probabilistic analysis if the 95% confidence interval on the correlation coefficient did not include

zero (Fisher's Z transformation on the correlation coefficient). The probability distribution of the stress predictions showed high variability, with the 5-95% cumulative probability range of stress about twice as high as the median stress (50% cumulative probability) in both directions, throughout the test (Figure 3.6). From the time at peak stress to 100 s of relaxation, there was an 11% increase in the variability (calculated as the 5-95% range, divided by the median stress), indicating that the large majority of the variability appears during the ramping period, and the long-term time-dependent behavior adds very little contribution to this variability. The global sensitivities of the model variance to the input parameter variance demonstrate that the model is most sensitive to the instantaneous elastic parameters early in the relaxation period of the test (Figure 3.7). As the relaxation time increases, the model becomes more sensitive to the variability of the G_1 and G_2 parameters. The G_3, G_4, and G_∞ parameters had negligible contributions to the model variance.

Table 3.2: Pearson's correlation coefficient between each model parameter for use in the probabilistic analysis.

	G_1	**G_2**	**G_3**	**G_4**	**G_∞**	**μ**	**α**	**k**
G_1	1	X	X	X	X	X	X	X
G_2	-0.93	1	X	X	X	X	X	X
G_3	0	0	1	X	X	X	X	X
G_4	-0.79	0.65	0	1	X	X	X	X
G_∞	-0.86	0.62	0	0.83	1	X	X	X
μ	0	0	0	0	0	1	X	X
α	0	0	0	0	0	0	1	X
k	0	0	0	0	0	-0.8	0	1

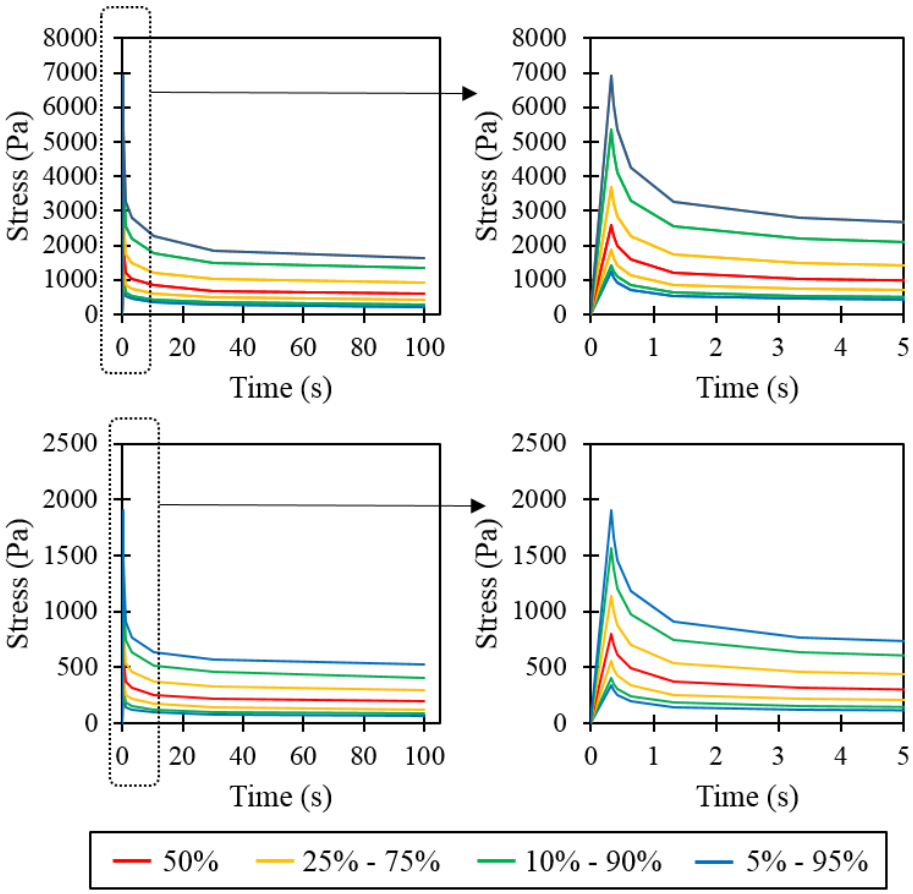

Figure 3.6: Probability distributions of the model stress predictions for an equibiaxial stress-relaxation test with a peak stretch of 1.1. Stress predictions are shown for the axonal direction (top) and transverse direction (bottom).

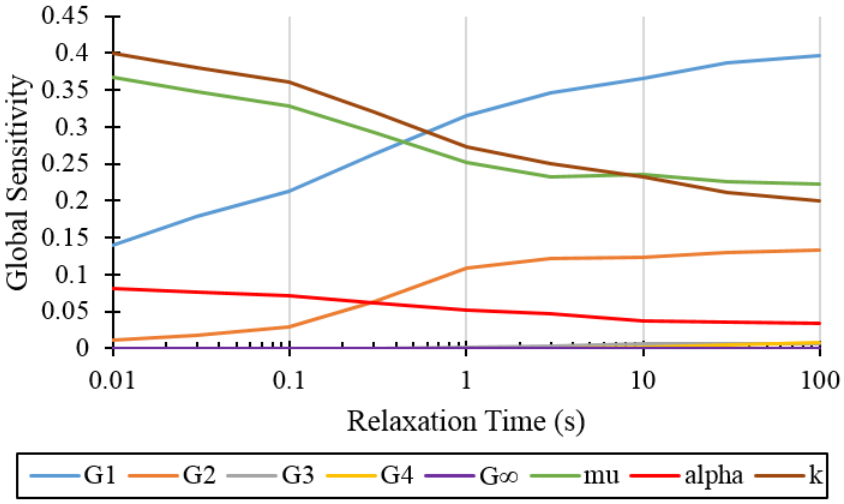

Figure 3.7: Global sensitivities of the model axonal stress prediction to the variance of the model parameters during the relaxation period of an equibiaxial stress-relaxation test.

3.4 Discussion

The viscoelastic properties of brain white matter were characterized by conducting equibiaxial stress-relaxation experiments at five different displacement magnitudes and determining the appropriate model formulation to fit the viscoelastic behavior. The results demonstrated that the time-dependent behavior of the tissue was independent of strain magnitude, therefore a QLV formulation was sufficient. QLV formulations have commonly been used to study brain viscoelasticity [Elkin et al. 2011, Laksari et al. 2012, Nicolle et al. 2004, Rashid et al. 2014, Tamura et al. 2007], however, systematic characterizations of the strain magnitude dependence are limited. Experiments in shear [Nicolle et al. 2004] and indentation [Elkin et al. 2011] provide evidence that relaxation behavior is independent of strain, supporting the results of the current study. Other soft tissues such as tendons [Troyer and Puttlitz 2011] and spinal cord [Shetye et al. 2014] have exhibited fully nonlinear viscoelastic behavior in tension. However, these tissues contain collagen fiber components, including the pia mater attached to the spinal cord, which may contribute to the nonlinearity of the relaxation behavior.

Previous viscoelastic studies of the brain have investigated the anisotropy of the elastic behavior or of the linear relaxation modulus [Abrogast and Margulies 1999, Feng et al. 2013, Nicolle el al. 2004, Ning et al. 2006]. However, the specific anisotropy of the time-dependent response has not been determined separately from the elastic behavior. In the current study, the hyperelastic component of mechanical response demonstrated strong anisotropy, with the k parameter ranging from 0.86 to 5.9 for the tested specimens. However, the time-dependent behavior (relaxation) was nearly the same in the axonal and transverse directions. The differences in the relaxation function parameters in the two directions were fairly small (less than a 10% difference). Although some of the differences in parameters were statistically significant,

they did not have a great enough effect on the model results to be meaningful. When a single, isotropic reduced relaxation function was used, the model fits remained accurate. It was therefore sufficient to use one single reduced relaxation function to define all terms of the reduced relaxation tensor.

QLV model coefficients are sometimes determined by fitting the reduced relaxation function to the relaxation period of the experiment only, assuming a Heaviside (instantaneous) strain application, and approximating the instantaneous elastic stress by fitting to a high speed ramp while assuming any relaxation that occurs during the ramp time is negligible [Rashid et al. 2014]. However, models determined by this method result in poor predictions of the experimental data when the actual strain history is taken into account [Abramowitch and Woo 2004, Troyer et al. 2012a]. A Heaviside fitting method was used in the current study (the resulting reduced relaxation function parameters are shown in Figure 3.3) and the parameters describing the instantaneous elastic stress were μ = 1400 ± 560 Pa, α = 19 ± 6.7, and k = 2.3 ± 1.6 (mean ± standard deviation). Some of these parameters are substantially different than those determined by the full-integral fitting method. Notably, G_1 is much greater, G_∞ is much smaller, and μ is much greater for the full-integral fitting. Consequentially, the test predictions based on the Heaviside fits were very inaccurate compared to the full-integral fits (Figure 3.8). The discrepancy arises due to the distinctly different relaxation behaviors predicted by the two models. By taking into account the actual strain history, the full-integral fits were able to accurately predict both the ramping and relaxation periods of the stress-relaxation experiments and the stresses in the cyclic experiments.

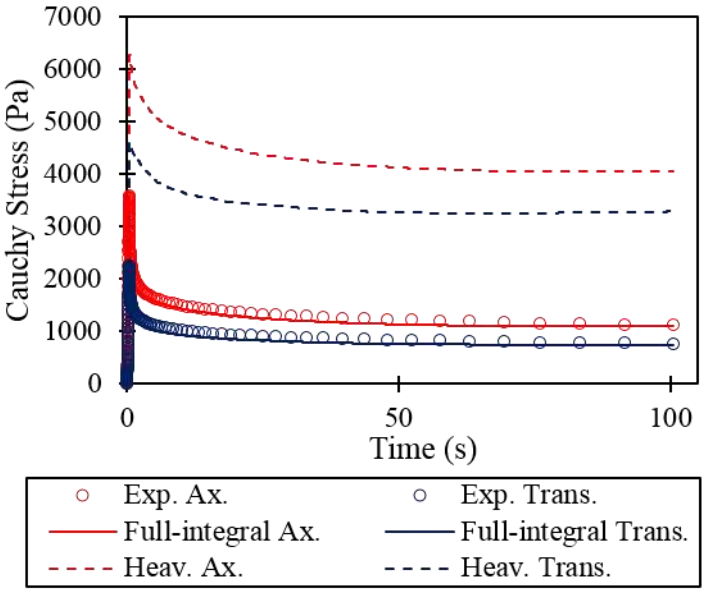

Figure 3.8: Predictions of the experimental stress-relaxation in the axonal and transverse directions based on fits using a Heaviside ramp assumption and fit full-integral fits taking into account the actual measured strain history.

The instantaneous elastic stress determined by the full-integral model had an infinitesimal shear modulus (μ = 3400 Pa) that is similar to what has been previously reported for high speed tensile stress relaxation tests of brain tissue [Rashid et al. 2014], which used strain rates of 30 – 90 s^{-1}, and reported means of 2780-5160 Pa for μ. Based on this comparison, the instantaneous shear modulus from the current study is a good approximation of the shear modulus at a strain rate of 60 s^{-1}. However, the model used by [Rashid et al. 2014] has a lower α parameter (α = 6) and no anisotropic parameter. Also, the reduced relaxation function determined in the current study may not give a reliable prediction of the relaxation that occurs in very short times at greater strain rates. The modeled instantaneous elastic response was much stiffer than the modeled hyperelastic behavior for previous quasi-static biaxial experiments using the same experimental setup (μ = 460 ± 270 Pa, α = 24 ± 6, and k = 0.54 ± 0.83) [Labus and Puttlitz 2016]. The same hyperelastic Ogden model was fitted to the stress-stretch data at 100 s of relaxation for the five tests to approximate the static material properties. The infinitesimal shear modulus was

very similar to that found from the quasi-static experiments ($\mu = 430 \pm 200$), but α (18 ± 3.6) and k (2.0 ± 1.5) were more similar to the instantaneous elastic properties from the current study. Differences in the anisotropy and nonlinearity may be due to the use of only equibiaxial tests in the current study, whereas the quasi-static experiments used multiple biaxial displacement ratios. In a model of uniaxial tension tests on white matter, a similar anisotropic parameter of $k = 1.77$ was found [Velardi et al. 2006].

The distributions of the model parameters lead to a high variability in predicted stresses in the probabilistic analysis. The model predictions were most sensitive to the variance of μ, k, and G_1 (Figure 3.7), so the majority of the model uncertainty arises from uncertainty in the elastic and early-time relaxation behavior. Conversely, the long-term relaxation behavior from the experiments was extremely consistent, as demonstrated by the negligible contributions of the long-term relaxation parameters to the model variance. The variability of the experimental data can be important to consider in computational studies in order to predict the full range and probability levels of model outcomes rather than only predicting the mean (Laz and Browne 2010). The reported distributions of the model parameters (Table 3.1) and their correlations (Table 3.2) can be implemented into probabilistic analyses of computational models similar to the probabilistic analysis conducted on the constitutive model.

The experimental stress was estimated by multiplying a correlation factor by the initial stress calculation of force divided by cross sectional area. This correlation factor was determined using specimen-specific finite element analyses, and it depends on the degree of anisotropy, the direction, and the magnitude of strain. Each direction of stress for each specimen had an independent correlation factor applied, with means of 0.78 in the axonal direction and 0.71 in the transverse direction. All modeling results reported above used the correlation factors,

however, the fits to the mean experimental data were repeated without the correlation factors. Because the correlation factors only affect the magnitude of the stress, and not the shape of the curves, the α parameter and the reduced relaxation function parameters were all identical using both methods. Without the correlation factors, μ increased to 4800 Pa (from 3400 Pa), and k decreased to 1.6 (from 1.9).

In conclusion, an anisotropic, viscoelastic constitutive model was derived from biaxial stress-relaxation tests on brain white matter. A QLV formulation was sufficient to model the relaxation behavior, which was independent of strain magnitude. Although the instantaneous elastic response was anisotropic, the time-dependent relaxation response was sufficiently modeled by an isotropic reduced relaxation function. Model fits to stress relaxation tests were able to accurately predict the stress in cyclic tests in both the axonal and transverse directions at two different strain magnitudes. The high variability in model stress predictions was due almost entirely to the variance of the elastic and the early-time relaxation parameters, whereas the long-term relaxation behavior was very consistent. The resulting constitutive model can be used to improve computational models of the brain used for surgical simulations.

4. CONCLUSION

4.1 Summary of Findings

A biaxial test of brain white matter was developed in this study to improve the constitutive models of brain tissue. Quasi-static experiments were conducted to determine the hyperelastic behavior of the tissue. Structural parameters were measured using histology and transmission electron microscopy imaging analyses. These parameters were incorporated into the hyperelastic constitutive model, and a probabilistic analysis was used to determine the improvements in the certainty of model predictions. Dynamic biaxial experiments were also conducted to tests the viscoelasticity of white matter and to derive the appropriate form of a viscoelastic model.

A novel experimental setup was developed to test brain tissue in biaxial tension, and this setup successfully minimized shear and created a relatively homogeneous region of interest to allow for an accurate analysis of white matter in a true state of biaxial tension. An anisotropic Ogden-type hyperelastic model was used to fit the experimental data, and the results showed a mean anisotropic behavior with the axonal direction stiffer than the transverse direction, although the degree of anisotropy was relatively low compared to previous studies of white matter. Model predictions showed improved accuracy when the model was fitted to all five experimental tests, compared to fitting to only the three biaxial tests or two uniaxial tests, indicating that using multiple strain ratios to derive the model parameters improves the predictive power of the model.

The results from the quasi-static experiments showed no significant differences in the mechanical model parameters between the corona radiata and corpus callosum regions. The

axon area fraction, measured via by transmission electron microscopy, also showed no significant differences between regions. However, results of the histology measurements showed both the mean axon orientation relative to the testing direction and the distribution of the axon orientation to be significantly greater in the corona radiata. From a regional perspective, differences in structural properties showed no relationship with the mechanical properties of white matter. However, when correlations were tested between mechanical model parameters and structural parameters on an individual specimen basis, a significant correlation was observed between the mechanical anisotropy and the axon area fraction. This correlation was accounted for in the structural hyperelastic model, and the variability of the axonal stress predictions decreased as a result. Because this correlation was seen only on an individual specimen basis, and not a regional basis, the utility of this modelling approach is applicable to patient-specific models. A more generally applicable model that is representative of the general population mean/median still needs to be developed and warrants further investigation.

The biaxial stress-relaxation experiments conducted at multiple equibiaxial strain magnitudes showed the time-dependent relaxation behavior to be independent of strain magnitude. Therefore, a QLV model was sufficient for modeling the experimental results. The relaxation was also nearly identical in the axonal and transverse directions, and an isotropic reduced relaxation tensor was able to accurately model both directions of stress in the biaxial stress-relaxation tests. A QLV model with an isotropic reduced relaxation tensor and an anisotropic instantaneous elastic stress was used to fit the stress relaxation tests and accurately predict the stress from cyclic tests at two different strain magnitudes. In order to obtain an accurate model, it was necessary to fit both the ramping and relaxation periods of the experiments simultaneously while taking into account the actual strain history of the tests.

4.2 Future Work

The constitutive models derived from quasi-static and dynamic biaxial experiments can be useful for computational modeling of surgical procedures, and the model selection may depend on specific requirements for the modeling application. While this work improves on the current models of brain tissue to describe multiaxial stress states, further investigations are warranted. Multiaxial stresses should be further tested in shear and compression. The structural modeling approach showed a limited ability to improve the certainty of model predictions. To further assess this approach, more information may be needed on the axonal structure of the brain, especially in comparing humans to animal models. In order to extend this work to model traumatic injuries, testing at higher strain rates would be required.

Tension, compression, and shear are all relevant in clinical applications of brain computational models. Moreover, the current study demonstrated the importance of conducting biaxial tensile tests in addition to uniaxial tests for deriving constitutive models with better predictive capabilities. This work could be extended to also test brain tissue mechanics in other multiaxial stress states that include compression and shear. Constitutive models could be further improved by simultaneously fitting to multiple experimental tests that include tension, compression, and shear in multiaxial stress states.

The axonal structural properties of the brain and their relation to mechanical behavior could be further investigated. A correlation was found between axon volume fraction and mechanical anisotropy on an individual specimen basis. While no significant differences were observed between the two regions testes, previous studies have found differences in mechanical behavior between regions of the brain. The relationship between axon volume fraction and anisotropy could be further investigated beyond the two regions tested in the current study. This

approach could also be used to study the differences in mechanical behavior between species, especially between humans and the commonly used ovine and porcine animal models. A systematic characterization of the axon structure of these species is warranted, alongside a mechanical characterization. Differences in the axon structure may account for interspecies differences in mechanical behavior. This approach would provide improved translation of the many animal models of brain mechanics to the human condition.

The current experiments were designed to develop models of the brain for use in clinical applications, such as surgical simulations. Therefore, relatively low strain rates were used. In order to extend this work to study traumatic brain injuries, higher strain rates should be used to characterize the viscoelastic behavior. However, mechanical tests at high loading rates have associated errors due to inertial effects of the specimen and the testing apparatus. These errors include out-of-plane stresses, inhomogeneous strains, and vibrations (Sanborn et al. 2012, Abramowich and Woo 2004). It is therefore important to develop testing methods that can minimize these errors. For modeling stress relaxation tests at high speeds, it remains important to measure the actual strain history, as done in the current study, rather than making assumptions about the loading profile. It is unclear if a quasi-linear viscoelastic model would still be sufficient for modeling white matter at high strain rates, accordingly, a systematic investigation of the strain magnitude dependence of the viscoelastic behavior should be conducted.

REFERENCES

Abramowitch SD and Woo SLY. (2004). "An improved method to analyze the stress relaxation of ligaments following a finite ramp time based on the quasi-linear viscoelastic theory." J. Biomech. Eng. 126(1): 92-97.

Abrogast KB, Margulies SS. (1999). "A fiber-reinforced composite model of the viscoelastic behavior of the brainstem in shear." J. Biomech. 32,865-870.

Allen NJ and Barres BA. (2009). "Glia – more than just brain glue." Nature. 457, 675-677.

Asher R, Perides G, Vanderhaeghen JJ, Bignami A. (1991). "Extracellular Matrix of Central Nervous System White Matter: Demonstration of an Hyaluronate-Protein Complex." J Neuroscience Research. 28,410-421.

Back SA, Riddle A, Dean J, Hohimer AR. (2012). "The instrumented fetal sheep as a model of cerebral white matter injury in the premature infant." Neurotherapeutics. 9,359-370.

Bain AC, Meaney DF. (2000). "Tissue-Level Thresholds for Axonal Damage in an Experimental Model of Central Nervous System White Matter Injury." J Biomech Eng. 122,615-622.

Bain AC, Shreiber DI, Meaney DF. (2003). "Modeling of Microstructural Kinematics During Simple Elongation of Central Nervous System Tissue." J. Biomech. Eng. 125, 708-804

Baldwin MA, Laz PJ, Stowe JQ, Rullkoetter PJ. (2009). "Efficient probabilistic representation of tibiofemoral soft tissue constraint." Comp Methods in Biomech and Biomed Eng. 12(6),651-659.

Bastacky J, Hayes TL, Gelinas RP. (1985). "Quantitation of shrinkage during preparation for scanning electron mocroscopy: Human lung." Scanning. 7, 134-140.

Bischoff JE, Arruda EM, Grosh K. (2004). "A rheological network model for the continuum anisotropic and viscoelastic behavior of soft tissue." Biomechan Model Mechanobiol. 3,56-65.

Catani M, Howard RJ, Pajevic S, Jones DK. (2002). "Virtual in Vivo Interactive Dissection of White Matter Fasciculi in the Human Brain." NeroImage. 17,77-94.

Chan S, Conti F, Salisbury K, Blevins N. (2013). "Virtual Reality Simulation in Neurosurgery: Technologies and Evolution." Neurosurgery. 72,A154-A164.

Cheng S, Bilston LE. (2007). "Unconfined compression of white matter." J Biomech. 40,117-124.

Cheng S, Clarke EC, Bilston LE. (2008). “Rheological properties of the tissues of the central nervous system: A review.” Medical Eng & Physics. 30,1318-1337.

Cheng S, Clarke EC, Bilston LE. (2009). “The effects of preconditioning strain on measured tissue properties.” J Biomech. 42,1360-1362.

Colgan NC, Gilchrist MD, Curran KM. (2010). “Applying DTI white matter orientations to finite element head models to examine diffuse TBI under high rotational accelerations.” Progress in Biophysics and Mol Bio. 103,304-309.

Cragg B. (1979). “Brain extracellular space fixed for electron microscopy.” Neuroscience Letters. 15,301-306.

Debanne D, Campanac E, Bialowas A, Carlier E, Alcaraz G. (2011). “Axon Physiology.” Physiol Rev. 91,555-602.

Duenwald SE, Vanderby Jr R, Lakes RS. (2009). “Viscoelastic relaxation and recovery of tendon.” Annals of Biomed. Eng. 37(6): 1131-1140.

Duncan J, Cock M, Scheerlinck J-P, Westcott K, McLean C, Harding R, Rees S. (2002). “White matter injury after repeated endotoxin exposure in the preterm ovine fetus.” Pediatric Res. 52(6),941-949.

Elkin BS, Ilankova A, Morrison III B. (2011). “Dynamic, Regional Mechanical Properties of the Porcine Brain: Indentation in the Coronal Plane.” J Biomech Eng. 133,071009.

Feng Y, Okamoto RJ, Namani R, Genin GM, Bayly P. (2013). “Measurements of mechanical anisotropy in brain tissue and implications for transversely isotropic material models of white matter.” J of Mech Behavior of Biomed Mat. 23,117-132.

Ferrant M, Nabavi A, Macq B, Jolesz F, Kikinis R, Warfield S. (2001). “Registration of 3-D Intraoperative MR Images of the Brain Using a Finite-Element Biomechanical Model.” IEEE Trans. Med. Imag. 20(12),1384-1397.

Franceshini G, Bigoni D, Regitnig P, Holzapfel GA. (2006). “Brain tissue deforms similarly to filled elastomers and follows consolidation theory.” J of Mech and Physics of Solids. 54,2592-2620.

Fung YC. (1993). “Biomechanics: Mechanical Properties of Living Tissues.” 2nd ed. New York: Springer.

García JJ, Molano AB, Smith JH. (2012). “Description and Validation of a Finite Element Model of Backflow During Infusion Into a Brain Tissue Phantom.” J. Comput. Nonlinear Dynam. 8(1),011017-011017-8.

Garo A, Hrapko M, van Dommelen JAW, Peters GWM. (2007). "Towards a reliable characterization of the mechanical behavior of brain tissue: The effects of *post-mortem* time and sample preparation." Biorheology. 44,51-58.

Gasser TC, Ogden RW, Holzapfel GA. (2006). "Hyperelastic modelling of arterial layers with distributed collagen fibre orientations." J R Soc Interface. 3,15-35.

Gefen A, Gefen N, Zhu Q, Raghupathi R, Margulies S. (2003). "Age-Dependent Changes in Material Properties of the Brain and Braincase of the Rat." J Neurotrauma. 20(11),1163-1177.

Gefen A, Margulies SS. (2004). "Are in vivo and in situ brain tissues mechanically similar?" J Biomech. 37,1339-1352.

Grashow JS, Sacks MS, Liao J, Yoganathan AP. (2006). "Planar biaxial creep and stress relaxation of the mitral valve anterior leaflet." Annals of Biomed Eng. 34(10): 1509-1518.

Green MA, Bilston LE, Sinkus R. (2008). "In vivo brain viscoelastic properties measured by magnetic resonance elastography." NMR Biomed. 21,755-764.

Hao H, Shreiber DI. (2007). "Axon Kinematics Change During Growth and Development." J Biomech Eng. 129,511-522.

Herculano-Houzel S. (2014). "The glial/neuron ratio: How it varies uniformly across brain structures and species and what that means for brain physiology and evolution." Glia. 62(9),1377-1391.

Holbourn AHS. (1943). "Mechanics of head injuries." The Lancet. 438-441.

Hrapko M, van Dommelen JAW, Peters GWM, Wismans JSHM. (2006). "The mechanical behavior of brain tissue: Large strain response and constitutive modelling." Biorheology. 43,623-636.

Hrapko M, van Dommelen JAW, Peters GWM, Wismans JSHM. (2008). "The Influence of Test Conditions on Characterization of the Mechanical Properties of Brain Tissue." J Biomech Eng. 130,031003.

Hursh JB. (1939). "Conduction velocity and diameter of nerve fibers." Am J of Physiology. 127,131-139.

Jacobs NT, Cortes DH, Vresilovic EJ, Elliott DM. (2013). "Biaxial Tension of Fibrous Tissue: Using Finite Element Methods to Address Experimental Challenges Arising From Boundary Conditions and Anisotropy." J Biomech Eng. 135,021004.

Jin X, Zhu F, Mao H, Shen M, Yang KH. (2013). "A comprehensive experimental study on material properties of human brain tissue." J Biomech. 46, 2795-2801.

Karami G, Grundman N, Abolfathi N, Naik Am Ziejewski M. (2009). "A micromechanical hyperelastic modeling of brain white matter under large deformation." J Mech Behavior Biomed Mat. 2,243-254.

Keller TS. (1994). "Predicting the compressive mechanical behavior of bone." J Biomech. 27(9),1159-1168.

Kim JHY, Ellman A, Juraska JM. (1996). "A re-examination of sex differences in axon density and number in the splenium of the rat corpus callosum." Brain Research. 740,47-56.

Kyriacou S, Mohamed A, Miller K, Neff S. (2002). "Brain Mechanics for Neurosurgery: Modeling Issues." Biomech Model Mechanobiol. 1,151-164.

Labus KM and Puttlitz CM. (2016). "An anisotropic hyperelastic constitutive model of brain white matter in biaxial tension and structural-mechanical relationships." J. Mech. Behav. Biomed. Mat. (In Press, DOI: 10.1016/j.jmbbm.2016.05.003).

Laksari K, Shafieian M, Darvish K. (2012). "Constitutive model for brain tissue under finite compression." J Biomech. 45,642-646.

Lau LW, Cua R, Keough MB, Haylock-Jacobs S, Yong VW. (2013). "Pathology of the brain extracellular matrix: a new target for remyelination." Nat Rev Neuosci. 14(10),722-729.

Laz PJ, Stowe JQ, Baldwin MA, Petrella AJ, Rullkoetter PJ. (2007). "Incorporating uncertainty in mechanical properties for finite element-based evaluation of bone mechanics." J Biomech. 40,2831-2836.

Laz PJ, Browne M. (2010). "A review of probabilistic analysis in orthopaedic biomechanics." Proc Inst Mech Eng H. 224(8),927-943.

Lippert SA, Rang EM, Grimm MJ. (2004). "The high frequency properties of brain tissue." Biorheology. 41(6),681-691.

Manduca A, Oliphant TE, Dresner MA, Mahowald JL, Kruse SA, Amromin E, Felmlee JP, Greenleaf JF, Ehman RL. (2001). "Magnetic resonance elastography: Non-invasive mapping of tissue elasticity." Medical Image Analysis. 5,237-254.

Meaney DF. (2003). "Relationship between structural modeling and hyperelastic material behavior: application to CNS white matter." Biomechan Model mechanobiol. 1,279-293.

Miller K, Chinzei K. (1997). "Constitutive modelling of brain tissue: experiment and theory." J Biomech. 30(11/12),1115-1121.

Miller K, Chinzei K, Orssengo G, Bednarz P. (2000). "Mechanical properties of brain tissue in-vivo: experiment and computer simulation." J Biomech. 33,1369-1376.

Miller K, Chinzei K. (2002). “Mechanical properties of brain tissue in tension.” J Biomech. 35,483-490.

Miller, K., Wittek, A., Joldes, G., Horton, A., Dutta-Roy, T., Berger, J. and Morriss, L. (2010). “Modelling brain deformations for computer-integrated neurosurgery.” Int. J. Numer. Meth. Biomed. Engng., 26: 117–138.

Miller K. (2011). “Biomechanics of the Brain” New York: Springer.

Moran R, Smith JH, García JJ. (2014). “Fitted hyperelastic parameters for Human brain tissue from reported tension, compression, and shear tests.” J Biomech. 47, 3762-3766.

Nagatomi J, Gloeckner DC, Chancellor MB, DeGroat WC, Sacks MS. (2004). “Changes in the Biaxial Viscoelastic Response of the Urinary Bladder following Spinal Cord Injury.” Annals Biomed Eng. 32(10),1409-1419.

NESSUS Theoretical Manual. (2014). Southwest Research Institute, San Antonia, Texas.

NESSUS User Manual. (2014). Southwest Research Institute, San Antonia, Texas.

Nguyen TD, Jones RE, Boyce BL. (2008). “A nonlinear anisotropic viscoelastic model for the tensile behavior of the corneal stroma.” J Biomech Eng. 130,041020.

Nicolle S, Lounis M, Willinger R. (2004). “Shear Properties of Brain Tissue over a Frequency Range Relevant for Automotive impact situations: New Experimental Results.” Stapp Car Crash J. 48,239-258.

Ning X, Zhu Q, Lanir Y, Margulies SS. (2006). “A Transversely Isotropic Viscoelastic Constitutive Equation for Brainstem undergoing Finite Deformation.” J Biomech Eng. 128,925-933.

Pan Y, Shreiber DI, Pelegri AA. (2011). “A Transition model for Finite Element Simulation of Kinematics of Central nervous System White Matter.” IEEE Trans Biomed Eng. 58(12),3443-3446.

Post A, Hoshizaki B, Gilchrist MD. (2012). “Finite element analysis of the effect of loading curve shape on brain injury predictors.” J Biomech. 45,679-683.

Prange MT, Margulies SS. (2002). “Regional, Directional, and Age-Dependent Properties of the Brain Undergoing Large Deformation.” J Biomech Eng. 124,244-252.

Prevost TP, Balakrishnan A, Suresh S, Socrate S. (2011). “Biomechanics of brain tissue.” Acta Biomaterialia. 7,83-95.

Rashid B, Destrade M, Gilchrist MD. (2012). “Mechanical characterization of brain tissue in compression at dynamic strain rates.” J Mech Behav Bioed Mater. 10,23-38.

Rashid B, Destrade M, Gilchrist MD. (2014). “Mechanical characterization of brain tissue in tension at dynamic strain rates.” J Mech Behav Biomed Mater. 33,43-54.

Sacks MS. (2000). “Biaxial Mechanical Evaluation of Planar Biological Mterials.” J. Elasticity. 61, 199-246.

Sacks MS. (2003). “Incorporation of Experimentally-derived Fiber Orientation into a Structural Constitutive Model for Planar Collagenous Tissues.” J Biomech Eng. 125,280-287.

Saher G, Brugger B, Lappe-Siefke C, Mobius W, Tozawa R, Wehr MC, Wieland F, Ishibashi S, Nave KA. (2005). “High cholesterol level is essential for myelin membrane growth.” Nature Neuroscience. 8,468-475.

Sanborn B, Nie X, Chen W, Weerasooriya T. (2012). “Inertia effects on characterization of dynamic response of brain tissue.” J. Biomech. 45: 434-439.

Sheleg SV, LoBello JR, Hixon H, Coons SW, Lowry D, Nedzved MK. (2008). “Stability and Autolysis of Cortical Neurons in Post-Mortem Adult Rat Brains.” Int J Clin Exp Pathol. 1, 291-299.

Shreiber DI, Hao H, Elias RA. (2009). “Probing the influence of myelin and glia on the tensile properties of the spinal cord.” Biomech Model Mechanobiol. 8,311-321.

Shetye SS, Troyer KL, Streijger F, Lee JHT, Kwon BK, Cripton PA, Puttlitz CM. (2014). “Nonlinear viscoelastic characterization of the porcine spinal cord.” Acta Biomaterialia. 10,792-797.

Shuck LZ, Advani SH. (1972). “Rheological Response of Human Brain Tissue in Shear.” J Fluids Eng. 94(4),905-911.

Silbereis JC, Huang EJ, Back SA, Rowitch DH. (2010). “Towards improved animal models of neonatal white matter injury associated with cerebral palsy.” Disease Models & Mechanisms. 3,678-688.

Smith and Garcia. (2013). “Constitutive Modeling of Brain Tissue using Ogden-type Strain Energy Functions.” Poromechanics V. 2140-2147.

Steiner LA, Andrews PJD. (2006). “Monitoring the injured brain: ICP and CBF.” British J Anaesthesia. 97(1),26-38.

Takhounts EG, Ridella SA, Tannous RE, Campbell Q, Malone D, Rowson S, Duma S. (2008). “Investigation of Traumatic Brain Injuries Using the Next Generation of Simulated Injury Monitor (SIMon) Finite Element head Model.” Stapp Car Crash J. 52,1-31.

Tamura A, Hayashi S, Watanabe I, Nagayama K, Matsumoto T. (2007). “Mechanical Characterization of Brain Tissue in High-Rate Compression.” J. Biomech. Science and Eng. 2(3): 115-126).

“The Internet Pathology Laboratory for Medical Education.” <http://library.med.utah.edu/WebPath/webpath.html#MENU>. 1994-2016, Edward C. Klatt MD, Savannah, GA, USA.

Troyer KL, Puttlitz CM. (2011). “Human cervical spine ligaments exhibit fully nonlinear viscoelastic behavior.” Acta Biomaterialia. 7,700-709.

Troyer KL, Estep DJ, Puttlitz CM. (2012a). “Viscoelastic effects during loading play an integral role in soft tissue mechanics.” Acta Biomaterialia. 8 234-243.

Troyer KL, Shetye SS, Puttlitz CM. (2012b). “Experimental Characterization and Finite Element Implementation of Soft Tissue Nonlinear Viscoelasticity.” J Biomech Eng. 134(11),114501.

Van Dommelen JAW, van der Sande TPJ, Hrapko M, Peters GWM. (2010). “Mechanical properties of brain tissue by indentation: Interregional variation.” J Mech Behav Biomed Mater. 3,158-166.

Velardi F, Fraternali F, Angelillo M. (2006). “Anisotropic constitutive equations and experimental tensile behavior of brain tissue.” Biomech Model Mechanbiol. 5,53-61.

Wakana S, Jiang H, Nagae-Poetscher LM, van Zijl PCM, Mori S. (2004). “Fiber Tract-based Atlas of Human White Matter Anatomy.” Radiology. 230,77-87.

Wang SSH, Shultz JR, Burish MJ, Harrison KH, Hof PR, Towns LC, Wagers MW, Wyatt KD. (2008). “Functional Trade-Offs in White Matter axonal Scaling.” J Neuroscience. 28(15),4047-4056.

Wright RM, Ramesh KT. (2012). “An axonal strain injury criterion for traumatic brain injury.” Biomech Model Mechanobiol. 11:245-260.

Xu G, Bayly PV, Taber LA. (2009). “Residual stress in the adult mouse brain.” Biomech Model Mechanobiol. 8,253-262.

Yuan A, Rao MV, Veeranna, Nixon RA. (2012). “Neurofilaments at a glance.” J Cell Sci. 125(Pt 14), 3257-3263.

Zhang L, Yang KH, King AI. (2001). “Comparison of Brain Responses Between Frontal and Lateral Impacts by Finite Element Modeling.” J Neurotrauma. 18(1),21-30.